Medicinal Chemistry Research (2019) 28:1838–1863
https://doi.org/10.1007/s00044-019-02418-1

MEDICINAL CHEMISTRY RESEARCH

ORIGINAL RESEARCH

Chemical synthesis, molecular modeling and pharmacophore mapping of new pyrrole derivatives as inhibitors of InhA enzyme and *Mycobacterium tuberculosis* growth

Shrinivas D. Joshi[1] · S. R. Prem Kumar[1] · Sonali Patil[1] · M. Vijayakumar[1] · Venkatarao H. Kulkarni[1] · Mallikarjuna N. Nadagouda[1] · Aravind M. Badiger[2] · Christian Lherbet[3] · Tejraj M. Aminabhavi[1]

Received: 12 March 2019 / Accepted: 1 August 2019 / Published online: 17 August 2019

Abstract

Substituted phenylthiazolyl benzamide and pyrrolyl benzamide derivatives were developed using molecular hybridization technique to create novel lead antimycobacterial molecules used to fight against *Mycobacterium tuberculosis*. The newly synthesized molecules have inhibited InhA, the enoyl-ACP reductase enzyme from the mycobacterial type II fatty acid biosynthetic pathway. Of these, compound **3b** showed H-bonding interactions with Tyr158 and co-factor NAD^+ that binds the active site of InhA. All the molecules were screened for in vitro antitubercular activity against *M. tuberculosis* $H_{37}Rv$, as well as some representative molecules as the inhibitors of InhA. Thirteen compounds exhibited good anti-TB activities (MIC = 1.6 µg/mL), but only few representative molecules showed the moderate InhA enzyme inhibition activity.

Supplementary information The online version of this article (https://doi.org/10.1007/s00044-019-02418-1) contains supplementary material, which is available to authorized users.

✉ Shrinivas D. Joshi
shrinivasdj@rediffmail.com

[1] Novel Drug Design and Discovery Laboratory, Department of Pharmaceutical Chemistry, S.E.T's College of Pharmacy, Sangolli Rayanna Nagar, Dharwad, Karnataka, India

[2] BDR Pharmaceuticals, Baroda, India

[3] Laboratoire de Syntheseet Physico-chimie de Molecules d'Interet Biologique, LSPCMIB, Universite de Toulouse, UPS, 118 Roote de Narbonne, F-31062 Toulouse Cedex 9, France

Graphical Abstract

Basic core moiety and docked mode of all the synthesized compounds inside the proposed binding pocket of InhA with the final selected pharmacophore model molecular alignment for InhA receptor ligands.

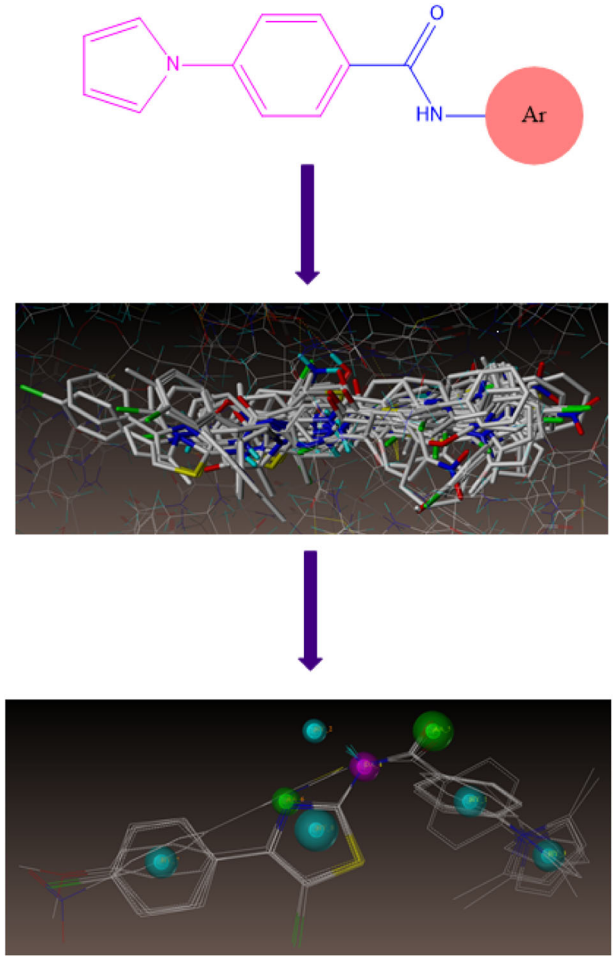

Keywords Pyrroles · Phenylthiazoles · Tuberculosis · *M. tuberculosis* $H_{37}Rv$ · Enoyl-ACP reductase · GALAHAD

Introduction

Mycobacterium tuberculosis (*M. tuberculosis*) has been the main widely spread contagious pathogen to cause tuberculosis (TB) among different strains of mycobacteria. As per the latest WHO report, TB is one of the most deadly diseases worldwide infecting nearly 10 million people with a death toll of 1.30 million among the common people and 0.3 million resulting from the TB cases co-infected with HIV. There is therefore an urgent need to fast-track the death rate of yearly decline by at least 4–5% by 2020 to achieve the milestones to eradicate the TB strategy. In recent years, multidrug-resistant TB (MDR-TB) and the emergence of rifampicin-resistant TB (RR-TB) have become more prominent. Consequently, TB remains to be the main public health threat attacking the lungs of the people along with other essential parts such as spine, kidney, and brain if not controlled properly on time (WHO 2019).

At present, there is an urgent need to develop novel chemotherapeutic agents to fight against TB, particularly multidrug and extensive drug resistance. Despite the availability of abundant innovative drugs for the treatment (Fig. 1), yet the drug-resistance still remains to be the challenging task. Therefore, there is a pressing need for developing more effective anti-TB agents with the activity against both MDR-TB and latent TB, which would help to reduce combined drug therapy. Recent trends towards targeted enzyme for testing novel anti-TB agents is InhA (Joshi et al. 2014), which is an enoyl acyl carrier protein reductase (ENR) from *M. tuberculosis* that is the main enzyme for type II fatty acid synthesis (FAS II), which catalyzes the reduction of 2-trans-enoyl-ACP

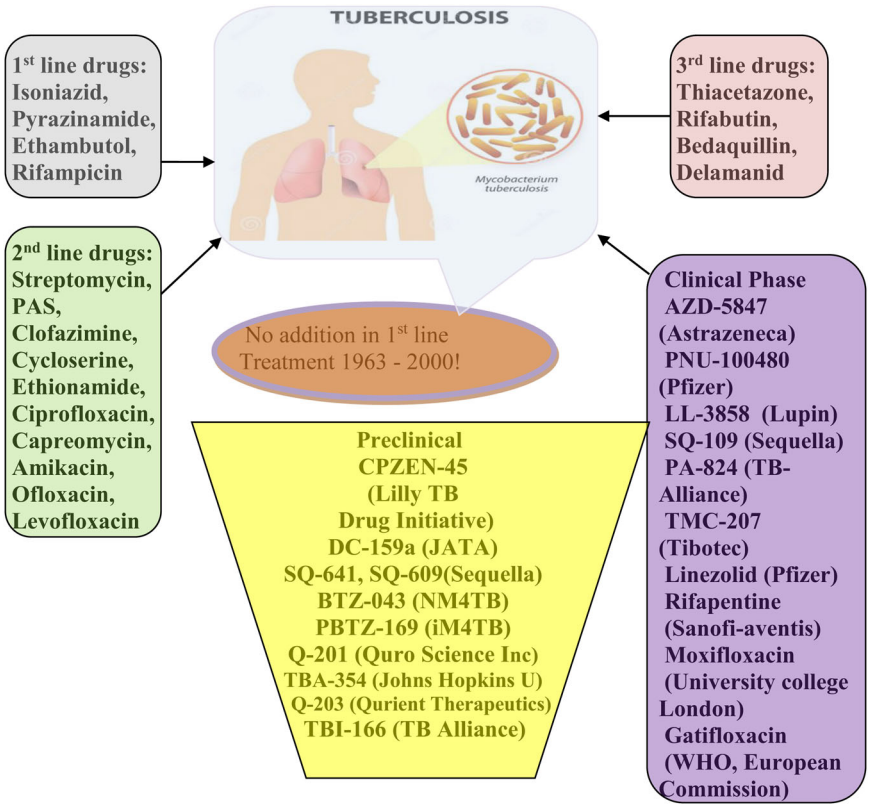

Fig. 1 Milestones in TB drug development research. *Abbreviations*: TB Tuberculosis, MDR multi-drug resistant, JATA Japan AntiTuberculosis Association, NM4TB new medicines for tuberculosis, iM4TB innovative medicines for tuberculosis

(acyl carrier protein) using NADH cofactor to give up NAD^+ and reduced enoyl thioester-ACP substrate; this in turn, aids the synthesis of mycolic acid that is the specific and essential constituent of mycobacterial envelope present in the FAS system of *M. tuberculosis*. InhA is an excellent target as the FAS II system in bacteria is not present in the human systems.

Hantzsch et al. and others have reported earlier the synthesis of thiazoles (Hantzsch and Weber 1887; Metzger 1984). Thiazole moiety is a part of many potent pharmacologically active drugs, such as sulfathiazole (antimicrobial drug), tiazofurin (anticancer drug), and ritonavir (antiretroviral drug). Thiazole derivatives have various pharmacological and biological activities, such as antibacterial (Hoshino et al. 2002; Dighe et al. 2011), antitubercular (anti-TB) (Karuvalam et al. 2012; Shiradakar et al. 2007), antifungal (Chimenti et al. 2007), anti-HIV (Masuda et al. 2005), and anti-inflammatory (Kalkhambkar et al. 2007).

Pyrrole is another nitrogen-containing heterocyclic moiety present in plant (naturally occurring chlorophyll) as well as animal kingdom (Hemin and vitamin-B_{12}). Antimycobacterial activity of BM212, an analog of pyrroles, was first reported by Deidda et al. (1998). Almost immediately after this discovery, a number of analogs of BM212 have been reported (Biava et al. 2006). Based on these results, Lupin, Astra Zeneca, and many other companies have synthesized a series of pyrrole-containing compounds of which LL3858 is currently in pre-clinical stage used for the treatment of TB (Arora et al. 2004).

In this perspective and in continuation of our ongoing program of research to develop new antitubercular molecules, herein we report the design and synthesis of new pyrrole derivatives as direct inhibitors of enoyl ACP reductase InhA (Fig. 2) (Joshi et al. 2016a, 2017, 2018), which exhibited substantial anti-TB activities. On the basis of versatile chemotherapeutic and pharmacological prospective of thiazoles, pyrroles, and the importance of peptide linkage, novel chemical scaffolds having phenyl thiazole, pyrrole, and peptide linkages with both antimycobacterial and antibacterial properties are developed in this research.

Even though there are several likely molecules having important antimycobacterial potency that can act as inhibitors of enoyl-ACP reductase enzyme, but after bedaquilin and delamanid none of these have emerged as potential drugs because these are still in their premature stage and preclinical phase. Keeping in mind the above facts, we have undertaken a much broader study on molecular modeling, pharmacophore mapping and synthesis of direct inhibitors of enoyl-ACP reductase containing pyrrolyl thiazoles and pyrrolyl benzamides as the main core unit using in silico methods involving the GALAHAD (pharmacophore based on an automated computational alignment) technique along with Surflex-docking studies to identify enoyl-ACP reductase as the probable target for these derivatives. Using these

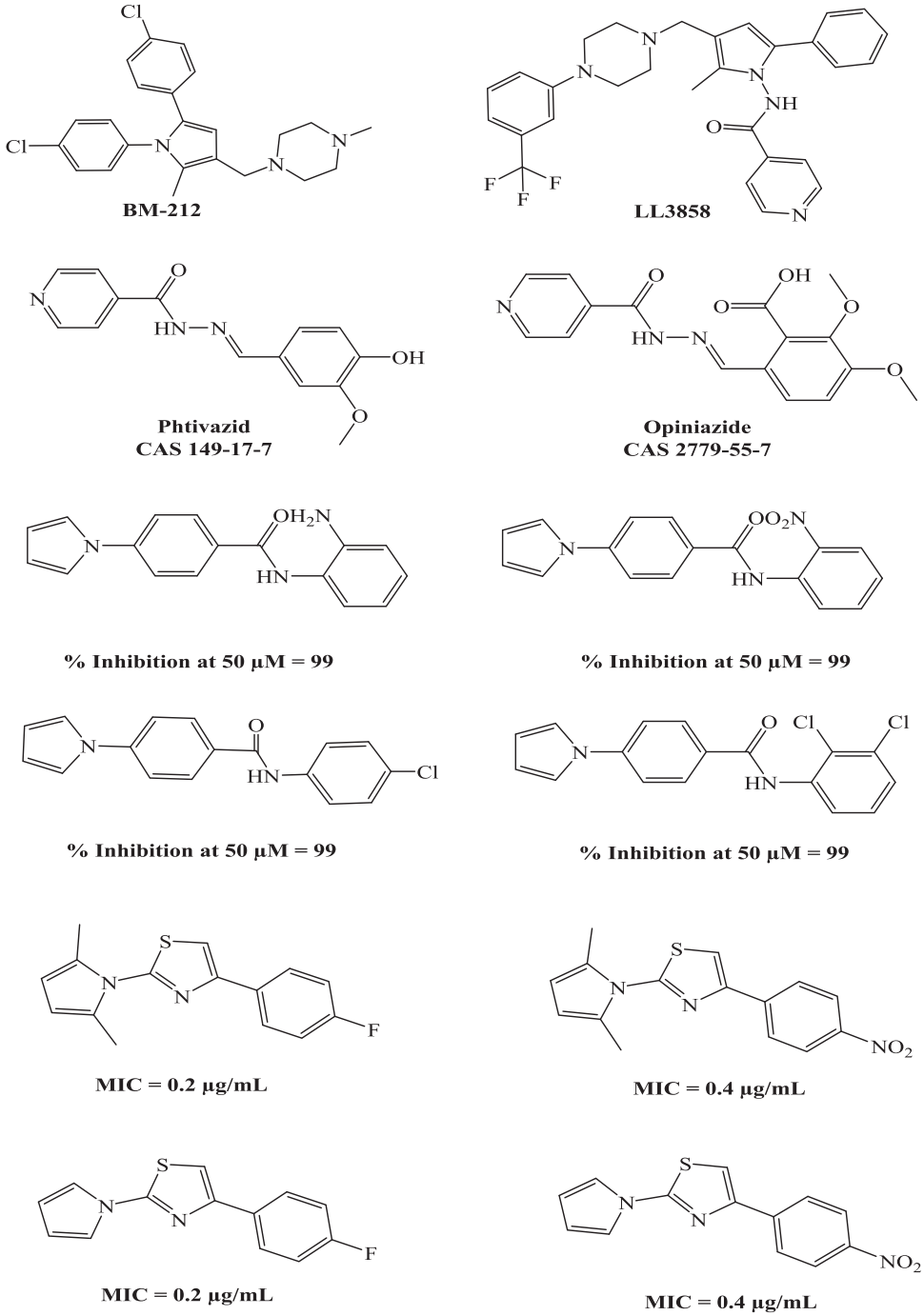

Fig. 2 Some antitubercular agents and our earlier reported pyrrole derivatives (Joshi et al. 2016a, 2017, 2018) having antitubercular and InhA inhibition activities

approaches, we have performed quantitative pharmacophore mapping method to identify the common functional groups accountable for the specific ligand–receptor interactions (Tropsha 2005) in conjunction with molecular-docking analysis on phenyl thiazole and pyrrole benzamide derivatives as the better InhA inhibitors and evaluated their bactericidal as well as antimycobacterial activities.

It is well known that compounds with amino thiazole and benzamide have displayed immpressive antimycobacterial activities, inhibiting the bacteria by targeting InhA (Guardia et al. 2016). Therefore, new antimycobacterial compounds are designed in this study with pyrrolyl thiazole and pyrrole benzamide nucleus by means of hybridization approach. In this perspective, we report here the essential pharmacophoric features derived from the basic structure of *N*-(4-methylbenzoyl)-4-benzylpiperidine, containing carbonyl H-bond acceptor and donor bridge between (4-benzylpiperidin-1-yl)(p-tolyl)methanone and 4-toluene, since they are acting as hydrophobic moieties. Hence, (4-benzylpiperidin-1-yl)(p-tolyl)methanone and 4-toluene were mapped

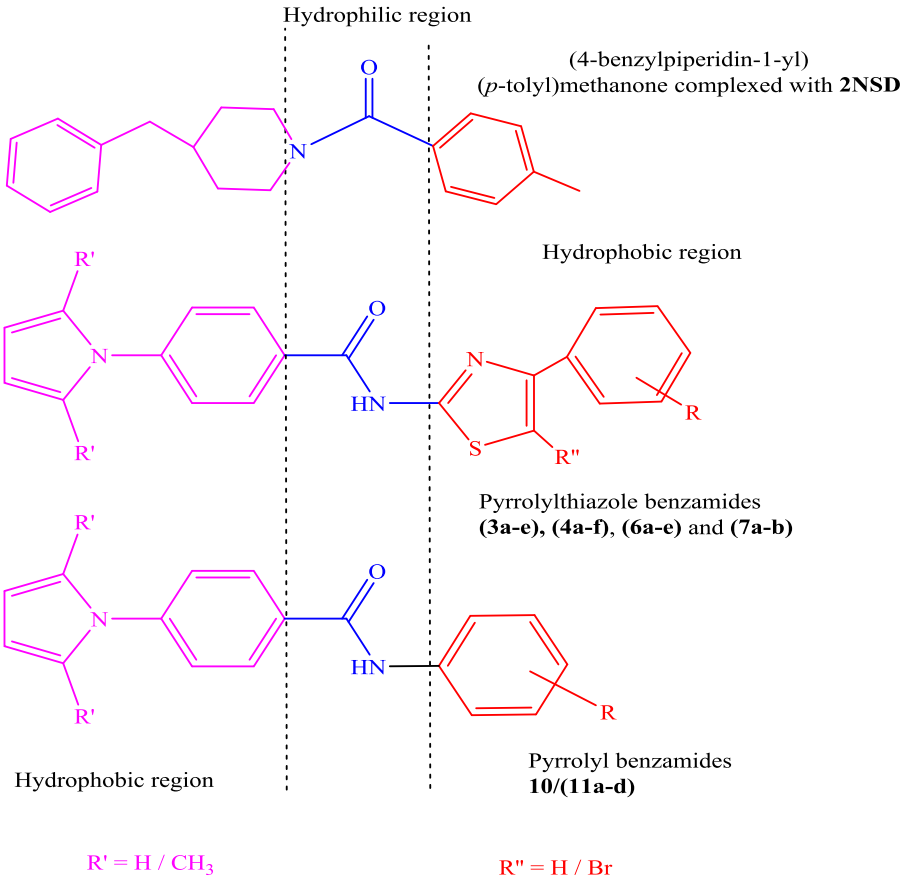

Fig. 3 Design concept used for the synthesis of titled compounds

with a carbonyl linkage (–CO–), which would allow possible interactions with the hydroxyl group of key residue Tyr158 and NAD+ of InhA (Chollet et al. 2015) and simultaneously hydrophobic moieties were mapped with o/m/p-substituted phenyl analogs of thiazole and pyrrole moieties as depicted in Fig. 3. These approaches were considered for the synthesis of new molecules using *Pall–Knorr* pyrrole synthesis (Joshi et al. 2016b). Hitherto, no such molecules have been explored in the literature and hence the reported compounds are novel.

Experimental

Materials and methods

Melting points were determined on a Shital-digital programmable melting point apparatus and are not corrected. Infrared spectra in KBr pellets were recorded on a Bruker FTIR spectrophotometer. The ^{1}H and ^{13}C NMR spectra were recorded on a Bruker AVANCE II at 400 and 100/75 MHz, respectively, using $CDCl_3$ or DMSO-d_6 as the solvent; chemical shifts are expressed in parts per million (δ ppm) relative to TMS. Abbreviations used to describe peak patterns are: (b) broad, (s) singlet, (d) doublet, (t) triplet, (q) quartet, (dd) doublet of doublet, (brs) broad singlet, (qu) quintet, and (m) multiplet.

Mass spectra (MS) were obtained on WATERS Q-Tof premier mass spectrometer and Schimadzu QP 20105 GC-mass spectrometer. Elemental analysis was done using TRUSPEC CHN analyzer. Analytical thin-layer chromatography (TLC) was performed on precoated TLC sheets of silica gel 60 F_{254} (Merck, Darmstadt, Germany) visualized by long-wavelength and short-wavelength UV lamps. Chromatographic purifications were performed on Merck aluminum oxide (70–230 mesh) and Merck silica gel (70–230 mesh). Purity of these compounds was confirmed by TLC analysis and their structures were confirmed by spectral studies.

General procedure for the synthesis of *N*-4-(4-substituted phenyl)thiazole-2-yl-4-(1*H*-pyrrol-1yl) bezamides (3a–e)/*N*-4-(4-substituted phenyl)thiazol-2-yl-4-(2,5-dimethyl-1*H*-pyrrol-1-yl)benzamides (4a–f)

The 2-amino-4-(4-substituted phenyl)thiazoles (**2a–f**) (Pattan et al. 2009) (0.0018 mol) and 4-(1*H*-pyrrolyl-1-yl)benzoic acid (**9a**) (Joshi et al. 2018)/4-(2,5-dimethyl-1*H*-pyrrolyl-1-yl)benzoic acid (**9b**) (Joshi et al. 2008) (0.0019 mol) were dissolved, respectively in 50 mL of dry

Scheme. 1 Synthesis of substituted thiazolyl pyrrolyl benzamides

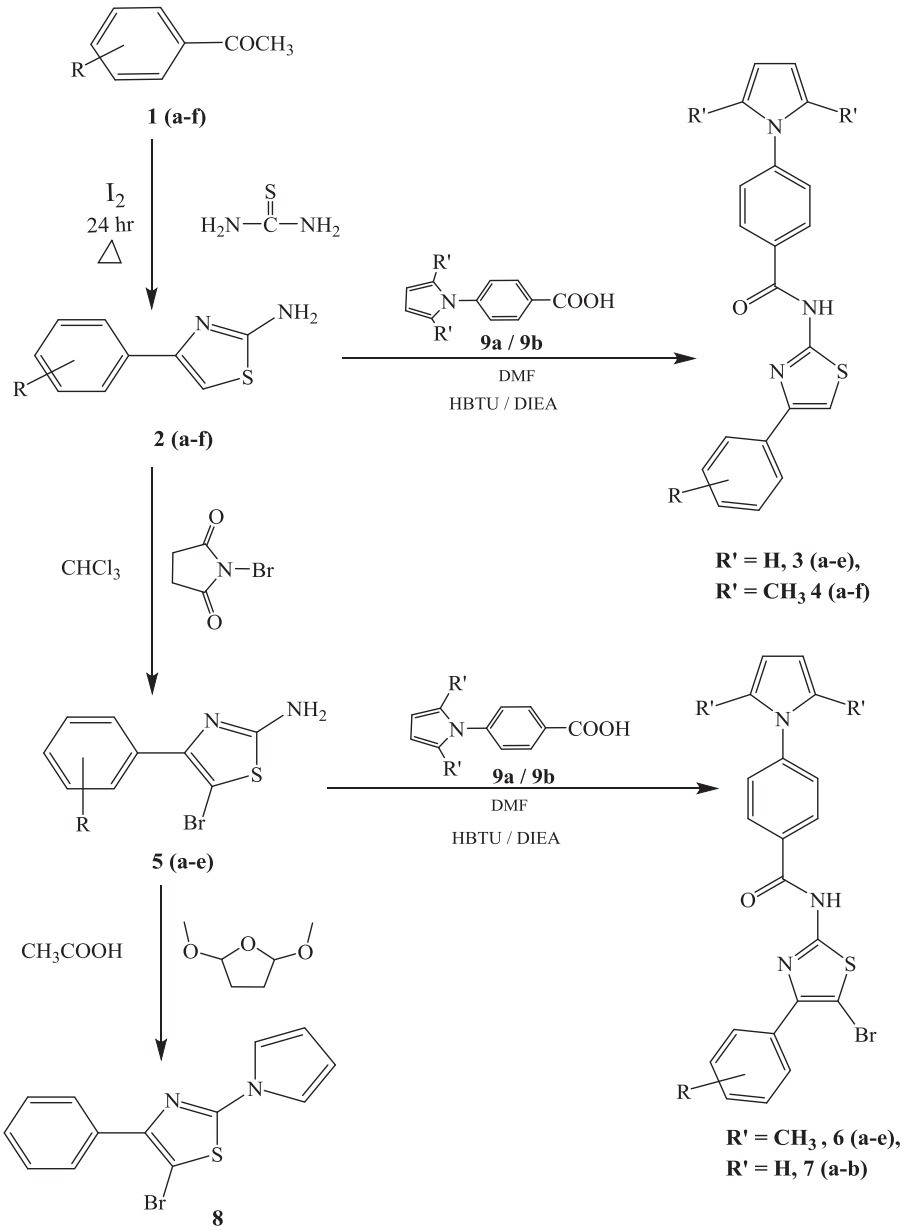

R = a) H, b) 4-Br, c) 4-Cl, d) 4-NO_2, e) 4-OCH_3, f) 3-Br.

R' = H / CH_3 = 9a / 9b

dimethyl formamide. HBTU (0.87 g, 0.0023 mol) and DIEA (0.93 mL, 0.0053 mol) were then added to the above mixtures and stirred for 24–30 h at ambient temperature. The reaction was quenched by adding NaCl solution and the mixture was extracted with ethyl acetate (3 × 50 mL). The combined ethyl acetate layer was washed with 1 N HCl and with a saturated sodium bicarbonate solution followed by NaCl. The organic layer was dried over anhydrous sodium sulfate and concentrated using a rotary flash evaporator. Thus obtained residue was dried and purified by column chromatography using petroleum ether:ethyl acetate (6:4) mixture as the eluent to afford the compounds (**3a–e**) and (**4–f**) (Scheme 1).

N-(4-phenyl-1,3-thiazol-2-yl)-4-(1H-pyrrol-1-yl)benzamide (3a)

Compound **3a** was obtained as yellow solid (yield 75%). m. p. 178–180 °C; FTIR (KBr): 3412, 3110, 1652, 1550 cm^{-1}. ^{1}H NMR (400 MHz, DMSO-d_6) δ ppm: 12.80 (1H, s, NH), 8.24 (2H, d, $J = 2.3$ Hz, H-16, H-20), 7.96 (2H, d, $J =$

5.4 Hz, H-17, H-19), 7.81 (2H, d, $J = 2.2$ Hz, H-10, H-14), 7.68 (1H, s, H-5), 7.43-7.32 (3H, m, H-11, H-12, H-13), 7.26 (2H, d, $J = 1.3$ Hz, H-22, H-25), 6.33 (2H, d, $J =$ 2.2 Hz, H-23, H-24). ^{13}C NMR (75 MHz, DMSO-d_6) δ ppm: 165.32 (CO, C-8), 162.77 (C-2), 150.32 (C-4), 144.83 (C-15), 131.70 (C-9), 130.51(C-18), 128.98 (CH, C-11,C-13), 128.73 (CH, C-16, C-20), 126.41 (CH, C-17, C-19), 126.26 (CH, C-10, C-14), 120.45 (CH, C-12), 118.02 (CH, C-23, C-24), 111.20 (CH, C-22, C-25), 101.22 (CH, C-5); MS (ESI): m/z = found 345.01 [M^+] (calcd. 345.42); Anal. Calcd. For $C_{20}H_{15}N_3OS$: C, 69.54; H, 4.38; N, 12.17; Found: C, 69.78; H, 4.62; N, 12.46.

N-[4-(4-bromophenyl)-1,3-thiazol-2-yl]-4-(1H-pyrrol-1-yl) benzamide (3b)

Compound **3b** was obtained as yellow solid (yield 70%). m.p. 166–168 °C; FTIR (KBr): 3418, 3114, 1612, 1527 cm^{-1}; ^{1}H NMR (400 MHz, DMSO-d_6) δ ppm: 12.81 (1H, s, NH), 8.24 (2H, d, $J = 8.7$ Hz, H-16, H-20), 7.91 (2H, d, $J = 1.8$ Hz, H-17, H-19), 7.76 (2H, d, $J = 2.4$ Hz, H-10, H-16), 7.62 (1H, s, H-5), 7.54 (2H, d, $J = 1.8$ Hz, H-11, H-13), 7.13 (2H, d, $J = 35.4$ Hz, H-23, H-26), 6.33 (2H, d, $J = 2.2$ Hz, H-24, H-25); ^{13}C NMR (75 MHz, DMSO-d_6) δ ppm: 168.39 (CO, C-8), 164.33 (C-2), 148.55 (C-4), 142.81(C-15), 140.23 (C-12), 133.51 (C-9), 131.63 (C-18), 130.84 (CH, C-11, C-13), 129.99 (CH, C-16, C-20), 127.96 (CH, C-10, C-14), 127.74 (CH, C-17, C-19), 118.94 (CH, C-24, C-25), 109.23 (CH, C-23, C-26), 102.34 (CH, C-5); MS (ESI): m/z = found 424.36 [M$^+$], 426.20 [M + 2] (calcd. 424.32); Anal. Calcd. For $C_{20}H_{14}BrN_3OS$: C, 56.61; H, 3.33; N, 9.90; Found: C, 57.01; H, 3.73; N, 10.10.

N-[4-(4-chlorophenyl)-1,3-thiazol-2-yl]-4-(1H-pyrrol-1-yl) benzamide (3c)

Compound **3c** was obtained as yellow solid (yield 69%). m. p. 190–192 °C; FTIR (KBr): 3436, 3113, 1607, 1528 cm^{-1}; ^{1}H NMR (400 MHz, DMSO-d_6) δ ppm: 12.81 (1H, s, NH), 8.24 (2H, d, $J = 8.7$ Hz, H-16, H-20), 8.01 (2H, d, $J =$ 8.4 Hz, H-10, H-14), 7.94 (2H, d, $J = 2.6$ Hz, H-17, H-19), 7.61 (1H, s, H-5), 7.55 (2H, d, $J = 2.0$ Hz, H-11, H-13), 7.36 (2H, d, $J = 2.0$ Hz, H-23, H-26), 6.33 (2H, d, $J =$ 2.0 Hz, H-24, H-25); ^{13}C NMR (75 MHz, DMSO-d_6) δ ppm: 168.33 (CO, C-8), 164.32 (C-2), 158.77 (C-4), 142.83 (C-15), 140.86 (C-12), 133.70 (C-9), 131.51 (C-18), 129.98 (CH, C-11, C-13), 128.73 (CH, C-16, C-20), 128.41 (CH, C-10, C-14), 127.45 (CH, C-17, C-19), 119.00 (CH, C-24, C-25), 111.39 (CH, C-23, C-26), 102.24 (C-5); MS (ESI): m/z = found 380.02 [M^+], 381.20 [M + 2] (calcd. 379.86); anal. calcd. For $C_{20}H_{14}ClN_3OS$: C, 63.24; H, 3.72; N, 11.06; Found: C, 63.61; H, 4.02; N, 11.44.

N-[4-(4-nitrophenyl)-1,3-thiazol-2-yl]-4-(1H-pyrrol-1-yl) benzamide (3d)

Compound **3d** was obtained as yellow solid (yield 52%). m. p. 194–196 °C; FTIR (KBr): 3398, 3147, 1603, 1513 cm^{-1}; ^{1}H NMR (400 MHz, DMSO-d_6) δ ppm: 12.62 (1H, s, NH), 8.22 (2H, d, $J = 8.9$ Hz, H-16, H-20), 8.09 (2H, d, $J =$ 8.7 Hz, H-17, H-20), 7.67 (1H, s, H-5), 7.55 (2H, d, $J =$ 2.4 Hz, H-10, H-14), 7.46 (2H, d, $J = 1.8$ Hz, H-11, H-13), 7.42 (2H, d, $J = 2.1$ Hz, H-24, H-25) 6.32 (2H, d, $J =$ 2.0 Hz, H-23, H-26); ^{13}C NMR (75 MHz, DMSO-d_6) δ ppm: 168.73 (CO, C-8), 149.93 (C-2), 146.50 (C-4), 143.32 (C-15), 141.23 (C-12), 139.92 (C-9), 131.09 (C-18), 129.59 (C-11, C-13), 126.94 (C-20, C-16), 125.22 (C-10, C-14), 124.76 (C-19, C-17), 118.10 (C-24, C-25), 110.33 (C-23, C-26), 105.65 (C-5); MS (ESI): m/z = found 390.62 [M^+] (calcd. 390.42); anal. calcd. For $C_{20}H_{14}N_4O_3S$: C, 61.53; H, 3.61; N, 14.35; Found: C, 61.73; H, 3.91; N, 14.65.

N-[4-(4-methoxyphenyl)-1,3-thiazol-2-yl]-4-(1H-pyrrol-1-yl) benzamide (3e)

Compound **3e** was obtained as yellow solid (yield 80%). m. p. 186–188 °C; FTIR (KBr): 3415, 3114, 1652, 1526 cm^{-1}; ^{1}H NMR (400 MHz, DMSO-d_6) δ ppm: 12.76 (1H, s, NH), 8.26 (2H, d, $J = 8.8$ Hz, H-11, H-13), 7.91 (2H, d, $J =$ 8.8 Hz, H-10, H-14), 7.80 (2H, d, $J = 8.8$ Hz, H-19, H-17), 7.56 (1H, s, H-5), 7.55 (2H, d, $J = 2.2$ Hz, H-20, H-16), 7.00 (2H, d, $J = 27.0$ Hz, H-23, H-26), 6.33 (2H, d, $J =$ 2.1 Hz, H-24, H-25), 3.80 (3H, s, H-21, OCH_3). ^{13}C NMR (75 MHz, DMSO-d_6) δ ppm: 168.73 (CO, C-8), 165.25 (C-2), 149.93 (C-4), 147.90 (C-15), 143.32 (C-9), 140.92 (C-18), 131.16 (C-12), 129.59 (C-11, C-13), 127.94 (C-16, C-20), 126.22 (C-10, C-14), 119.10 (C-17, C-19), 118.87 (C-24, C-25), 111.33 (C-23, C-26), 106.65 (C-5), 60.80 (C-21); MS (ESI): m/z = found 374.98 [M-1] (calcd. 375.45); Anal. Calcd. For $C_{21}H_{17}N_3O_2S$: C, 67.18; H, 4.56; N, 11.19; Found: C, 67.46; H, 4.78; N, 11.35.

4-(2,5-dimethyl-1H-pyrrol-1-yl)-N-(4-phenyl-1,3-thiazol-2-yl) benzamide (4a)

Compound **4a** was obtained as brown solid (yield 62%). m. p. 154–156 °C; FTIR (KBr): 3320, 2920, 1606, 1516 cm^{-1}; ^{1}H NMR (400 MHz, DMSO-d_6) δ ppm: 12.89 (1H, s, NH), 8.07 (2H, d, $J = 16.0$ Hz, H-16, H-20), 7.98 (2H, d, $J =$ 7.6 Hz, H-17, H-20), 7.80 (2H, d, $J = 8.0$ Hz,H-10, H-14), 7.70 (1H, s, H-5), 7.40–7.22 (3H, m, H-11, H-12, H-13), 5.85 (2H, d, $J = 7.6$ Hz, H-23, H-24), 2.02 (6H, s, H-26, H-27-diCH_3); ^{13}C NMR (75 MHz, DMSO-d_6) δ ppm: 168.73 (CO, C-8), 164.25 (C-2), 146.83 (C-4), 143.90 (C-15), 143.12 (C-12), 138.92 (C-9), 131.99 (C-18), 128.59 (CH, C-11, C-14), 125.94 (CH, C-16, C-20), 124.29 (CH, C-10,

C-14), 123.37 (CH, C-17, C-19), 119.20 (CH, C-23, C-24), 110.53 (CH, C-22, C-25), 105.85 (C-5), 13.45 (C-26,C-27-diCH$_3$); MS (ESI): m/z = found 373.97 [M$^+$] (calcd. 373.47); anal. calcd. For $C_{22}H_{19}N_3OS$: C, 70.75; H, 5.13; N, 11.25; Found: C, 70.98; H, 5.37; N, 11.47.

N-[4-(4-bromophenyl)-1,3-thiazol-2-yl]-4-(2,5-dimethyl-1H-pyrrol-1-yl)benzamide (4b)

Compound **4b** was obtained as brown solid (yield 70%). m.p. 98–100 °C; FTIR (KBr): 3304, 2924, 1608, 1515 cm^{-1}. ^{1}H NMR (400 MHz, DMSO-d_6) δ ppm: 11.45 (1H, s, NH), 8.14 (2H, d, J = 1.9 Hz, H-16, H-20), 7.89 (2H, d, J = 8.3 Hz, H-17, H-19), 7.53 (2H, d, J = 2.0 Hz, H-10, H-14), 7.54 (1H, s, H-5), 7.37 (2H, d, J = 3.2 Hz, H-11, H-13), 5.94 (2H, d, J = 6.4 Hz, H-24, H-25), 2.01 (6H, s, H-27, H-28-diCH$_3$); ^{13}C NMR (75 MHz, DMSO-d_6) δ ppm: 168.66 (CO,C-8), 163.55 (C-2), 146.33 (C-4), 143.20 (C-15), 142.02 (C-12), 138.32 (C-9), 130.65 (C-18), 129.11 (CH, C-11, C-13), 125.64 (CH, C-16, C-20), 123.27 (CH, C-10, C-14), 121.37 (CH, C-17, C-19), 119.20 (CH, C-24, C-25), 110.93 (CH, C-23, C-26), 105.55 (C-5), 13.65 (C-27, C-28-diCH$_3$); MS (ESI): m/z = found 452.17 [M$^+$], 454.07 [M + 2] (calcd. 452.37); anal. calcd. For $C_{22}H_{18}BrN_3OS$: C, 58.41; H, 4.01; N, 9.29; Found: C, 58.61; H, 4.39; N, 9.42.

N-[4-(4-chlorophenyl)-1,3-thiazol-2-yl]-4-(2,5-dimethyl-1H-pyrrol-1-yl)benzamide (4c)

Compound **4c** was obtained as brown solid (yield 55%). m.p. 162–164 °C; FTIR (KBr): 3312, 2923, 1607, 1516 cm^{-1}; ^{1}H NMR (400 MHz, DMSO-d_6) δ ppm: 12.91 (1H, s, NH), 8.26 (2H, d, H-16, H-20), 8.07 (2H, d, H-10, H-14), 7.81 (2H, d, H-17, H-19), 7.42 (1H, s, H-5), 7.12 (2H, d, H-11, H-13), 5.85 (2H, s, H-24, H-25), 2.00 (6H, s, H-27, H-28-diCH$_3$). ^{13}C NMR (75 MHz, DMSO-d_6) δ ppm: 169.33 (CO, C-8), 165.25 (C-2), 147.63 (C-4), 144.90 (C-15), 143.12 (C-12), 139.92 (C-9), 130.99 (C-18), 128.99 (CH, C-11, C-13), 125.24 (CH, C-16, C-20), 124.69 (CH, C-10, C-14), 123.97 (CH, C-17, C-19), 118.20 (CH, C-24, C-25), 111.53 (CH, C-23, C-26), 106.85 (C-5), 13.95 (C-27,C-28-diCH$_3$); MS (ESI): m/z = found 407.90 [M$^+$], 409.12 [M + 2] (calcd. 407.92); anal. calcd. For $C_{22}H_{18}ClN_3OS$: C, 64.78; H, 4.45; N, 10.30; Found: C, 64.96; H, 4.71; N, 10.68.

4-(2,5-Dimethyl-1H-pyrrol-1-yl)-N-[4-(4-nitrophenyl)-1,3-thiazol-2-yl]benzamide (4d)

Compound **4d** was obtained as brown solid (yield 65%). m.p. 106–108 °C; FTIR (KBr): 3316, 3067, 1714, 1517 cm^{-1}; ^{1}H NMR (400 MHz, DMSO-d_6) δ ppm: 14.02 (1H, s, NH), 8.31 (2H, d, J = 2.0 Hz, H-11, H-13), 8.17 (2H, d, J = 3.4 Hz, H-10, H-14), 8.11 (2H, d, J = 2.0 Hz, H-16, H-20), 7.56 (1H, s, H-5), 7.20 (2H, d, J = 4.0 Hz, H-17, H-19), 4.42 (2H, d, J = 1.2 Hz, H-24, H-25), 2.01 (6H, s, H-27, H-28-diCH$_3$). ^{13}C NMR (75 MHz, DMSO-d_6) δ ppm: 168.73 (CO, C-8), 164.25 (C-2), 146.83 (C-4), 143.90 (C-15), 143.12 (C-12), 138.92 (C-9), 131.99 (C-18), 128.59 (CH, C-11, C-13), 125.94 (CH, C-16, C-20), 124.29 (CH, C-10, C-14), 123.37 (CH, C-17, C-19), 119.20 (CH, C-24, C-25), 110.53 (CH, C-23, C-26), 105.96 (C-5), 13.45 (C-27,C-28-diCH$_3$); MS (ESI): m/z = found 418.00 [M$^+$] (calcd. 418.47); anal. calcd. For $C_{22}H_{18}N_4O_3S$: C, 63.14; H, 4.34; N, 13.39; Found: C, 63.44; H, 4.71; N, 13.49.

N-[4-(4-methoxyphenyl)-1,3-thiazol-2-yl]-4-(2,5-Dimethyl-1H-pyrrol-1-yl)benzamide (4e)

Compound **4e** was obtained as brown solid (yield 75%). m.p. 104–106 °C; FTIR (KBr): 3244, 3100, 1669, 1541 cm^{-1}; ^{1}H NMR (400 MHz, DMSO-d_6) δ ppm: 12.86 (1H, s, NH), 8.09 (2H, d, J = 8.4 Hz, H-16, H-20), 7.87 (2H, d, J = 8.1 Hz, H-17, H-19), 7.68 (2H, d, J = 2.0 Hz, H-10, H-14), 7.60 (1H, s, H-5), 7.45 (2H, d, J = 4.9 Hz, H-11, H-13), 5.85 (2H, d, J = 7.0 Hz, H-24, H-25), 2.32 (3H, s, H-21, OCH$_3$), 2.00 (6H, s, H-27, H-28-diCH$_3$); ^{13}C NMR (75 MHz, DMSO-d_6) δ ppm: 165.93 (CO, C-8), 164.05 (C-2), 150.83 (C-4), 142.90 (C-15), 132.12 (C-12), 131.30 (C-9), 130.92 (C-18), 129.99 (CH, C-11, C-13), 128.69 (CH, C-16, C-20), 125.94 (CH, C-10, C-14), 124.29 (CH, C-17, C-19), 123.37 (CH, C-24, C-25), 106.32 (CH, C-23, C-26), 105.20 (C-5), 21.23 (C-21, OCH$_3$), 13.08 (C-27,C-28, diCH$_3$); MS (ESI): m/z = found 387.44 [M$^+$] (calcd. 387.14); anal. calcd. For $C_{23}H_{21}N_3OS$: C, 71.29; H, 5.46; N, 10.84; Found: C, 71.62; H, 5.67; N, 11.04.

N-[4-(3-bromophenyl)-1,3-thiazol-2-yl]-4-(2,5-dimethyl-1H-pyrrol-1-yl)benzamide (4f)

Compound **4f** was obtained as brown solid (yield 68%). m.p. 84–86 °C; FTIR (KBr): 3452, 3118, 1673, 1523 cm^{-1}; ^{1}H NMR (400 MHz, DMSO-d_6) δ ppm: 12.88 (1H, s, NH), 8.07 (2H, d, J = 6.2 Hz, H-16, H-20), 7.99 (2H, d, J = 8.7 Hz, H-17, H-19), 7.72 (1H, s, H-5), 7.84–7.14 (4H, m, H-14, H-12, H-10, H-13), 5.84 (2H, d, J = 6.8 Hz, H-24, H-25), 2.01 (6H, s, H-27, H-28-diCH$_3$); ^{13}C NMR (75 MHz, DMSO-d_6) δ ppm: 166.33 (CO, C-8), 163.25 (C-2), 148.83 (C-4), 144.90 (C-15), 139.12 (C-12), 138.62 (C-9), 132.79 (C-18), 128.79 (CH, C-10, C-14), 125.75 (CH, C-16, C-20), 124.19 (C-11), 123.07 (CH, C-17, C-19), 120.20 (CH, C-24, C-25), 108.85 (CH, C-23, C-26), 105.54 (C-5), 14.46 (C-27,C-28-diCH$_3$); MS (ESI): m/z = found 452.26 [M$^+$], 454.06 [M + 2] (calcd. 452.33); anal. calcd. For $C_{22}H_{18}BrN_3OS$: C, 58.41; H, 4.01; N, 9.29; Found: C, 58.78; H, 4.37; N, 9.37.

General procedure for the synthesis of *N*-(5-bromo-4-(4-substitutedphenyl)-thiazol-2-yl)-4-(2,5-dimethyl-1*H*-pyrrol-1-yl)benzamides (6a-e)/*N*-(5-bromo-4-(4-substitutedphenyl)-thiazol-2-yl)-4-(1*H*-pyrrol-1-yl)benzamides (7a-b)

The 4-(4-substituted phenyl)-5-bromo-2-aminothiazoles (**5a–e**) (0.0018 mol) and 4-(2, 5-dimethyl-1*H*-pyrrol-1-yl)benzoic acid (**9b**)/4(1*H*-pyrrol-1-yl)benzoic acid (**9a**) (0.0019 mol) were dissolved, respectively in 50 mL of dry dimethyl formamide. HBTU (0.87 g, 0.0023 mol) and DIEA (0.93 mL, 0.0053 mol) were then added to the above mixtures and stirred for 24–30 h at room temperature. The reaction was quenched by adding NaCl solution and the mixture was extracted with ethyl acetate (3 × 50 mL). The combined ethyl acetate layer was washed with 1 N HCl and with a saturated sodium bicarbonate solution followed by NaCl. The organic layer was dried over anhydrous sodium sulfate and concentrated using a rotary flash evaporator. Thus obtained residue was dried and purified by column chromatography using petroleum ether:ethyl acetate (6:4) mixture as the eluent to afford the compounds (**6a–e**) and (**7a–b**) (Scheme 1).

N-(5-bromo-4-phenyl-1,3-thiazol-2-yl)-4-(2,5-dimethyl-1H-pyrrol-1-yl)benzamide (6a)

Compound **6a** was obtained as red solid (yield 86%). m.p. 108–110 °C; FTIR (KBr): 3298, 3178, 1708, 1607 cm^{-1}; ^1H NMR (400 MHz, DMSO-d_6) δ ppm: 12.10 (1H, s, NH), 8.08 (2H, d, $J = 8.4$ Hz, H-17, H-21), 7.91 (2H, d, $J = 3.7$ Hz, H-18, H-20), 7.82 (2H, d, $J = 6.7$ Hz, H-10, H-14), 7.78–7.20 (3H, m, H-11, H-12, H-13), 5.77 (2H, s, H-24, H-25), 2.00 (6H, s, H-27, H-28-diCH_3); ^{13}C NMR (75 MHz, DMSO-d_6) δ ppm: 168.19 (CO, C-8), 166.98 (C-2), 152.30 (C-4), 143.20 (C-16), 134.93 12 (C-12), 133.75 (C-9), 130.18 (C-19), 128.44 (CH, C-10, C-14), 128.15 (CH, C-17, C-21), 127.78 (CH, C-11, C-13), 127.15 (CH, C-18, C-20), 125.53 (CH, C-23, C-26), 108.69 (CH, C-24, C-25), 101.47 (C-5), 12.55 (C-27, C-28-diCH_3); MS (ESI): m/z = found 452.47 [M^+], 454.10 [M + 2] (calcd. 452.37); anal. calcd. For $C_{22}H_{18}N_3OSBr$: C, 58.41; H, 4.01; N, 9.29; Found: C, 58.69; H, 4.33; N, 9.52.

N-[5-bromo-4-(4-bromophenyl)-1,3-thiazol-2-yl]-4-(2,5-dimethyl-1H-pyrrol-1-yl)benzamide (6b)

Compound **6b** was obtained as red solid (yield 78%). m.p. 138–140 °C; FTIR (KBr): 3297, 2969, 1667, 1607 cm^{-1}; ^1H NMR (400 MHz, DMSO-d_6) δ ppm: 12.7 (1H, s, NH), 8.10 (2H, d, $J = 3.6$ Hz, H-17, H-21), 7.77 (2H, d, $J = 2.0$ Hz, H-18, H-20), 7.75 (2H, d, $J = 1.9$ Hz, H-10, H-14), 7.55 (2H, d, $J = 4.2$ Hz, H-11, H-13), 5.88 (2H, s, H-25, H-26), 1.99 (6H, s, H-28, H-29-diCH_3); ^{13}C NMR (75 MHz, DMSO-d_6) δ ppm: 167.19 (CO, C-8), 166.58 (C-2), 144.01 (C-4), 134.01 (C-16), 131.38 (C-12), 128.16 (C-9), 127.95 (C-19), 127.78 (CH, C-10, C-14), 127.15 (CH, C-17, C-21), 125.45 (CH, C-18, C-20), 124.23 (CH, C-11, C-13), 122.32 (CH, C-24, C-27), 108.69 (CH, C-25, C-26), 102.17 (C-5), 12.85 (C-28, C-29-diCH_3); MS (ESI): m/z = found 531.19 [M^+], 533.29 [M + 2], 535.09 [M + 4] (calcd. 531.27); anal. calcd. For $C_{22}H_{17}N_3OSBr_2$: C, 49.74; H, 3.23; N, 7.91; Found: C, 49.94; H, 3.57; N, 8.11.

N-[5-bromo-4-(4-chlorophenyl)-1,3-thiazol-2-yl]-4-(2,5-dimethyl-1H-pyrrol-1-yl)benzamide (6c)

Compound **6c** was obtained as red solid (yield 76%). m.p. 174–176 °C; FTIR (KBr): 3301, 2972, 1606 cm^{-1}; ^1H NMR (400 MHz, DMSO-d_6) δ ppm: 12.82 (1H, s, -NH), 8.04 (2H, d, $J = 8.7$ Hz, H-17, H-21), 7.84 (2H, d, $J = 8.7$ Hz, H-10, H-14), 7.57 (2H, d, $J = 9.7$ Hz, H-18, H-20), 7.17 (2H, d, $J = 9.4$ Hz, H-11, H-13), 5.85 (2H, d, $J = 7.3$ Hz, H-25, H-26), 2.01 (6H, s, H-28, H-29-diCH_3); ^{13}C NMR (75 MHz, DMSO-d_6) δ ppm: 167.29 (CO, C-8), 166.78 (C-2), 154.39 (C-4), 139.56 (C-16), 138.558 (C-12), 133.55 (C-9), 130.28 (C-19), 128.10 (CH, C-10, C-14), 128.00 (CH, C-17, C-21), 127.68 (CH, C-11, C-13), 124.43 (CH, C-18, C-20), 123.59 (CH, C-24, C-27), 109.09 (CH, C-25, C-26), 102.67 (C-5), 13.45 (C-28, C-29-diCH_3); MS (ESI): m/z = found 486.82 [M^+], 487.22 [M + 2], 490.08 [M + 4] (calcd. 486.81); anal. calcd. For $C_{22}H_{17}N_3OSBrCl$: C, 54.28; H, 3.52; N, 8.63; Found: C, 54.46; H, 3.69; N, 8.86.

N-[5-bromo-4-(4-nitrophenyl)-1,3-thiazol-2-yl]-4-(2,5-dimethyl-1H-pyrrol-1-yl)benzamide (6d)

Compound **6d** was obtained as red solid (yield 80%). m.p. 164–166 °C; FTIR (KBr): 3304, 3150, 1664, 1600 cm^{-1}; ^1H NMR (400 MHz, DMSO-d_6) δ ppm: 10.79 (1H, s, NH), 8.14 (2H, d, $J = 1.8$ Hz, H-17, H-21), 8.10 (2H, d, $J = 2.0$ Hz, H-18, H-20), 7.85 (2H, d, $J = 3.2$ Hz, H-10, H-14), 7.74 (2H d, $J = 6.9$ Hz, H-11, H-13), 5.85 (2H, d, $J = 2.4$ Hz, H-25, H-26), 2.01 (6H, s, H-28, H-29-diCH_3); ^{13}C NMR (75 MHz, DMSO-d_6) δ ppm: 168.90 (NH-CO), 168.60 (C-2), 147.82 (C-4), 145.91 (C-16), 140.87 (C-12), 129.52 (C-9), 128.73 (C-19), 127.59 (CH, C-10, C-14), 126.27 (CH, C-17, C-21), 124.00 (CH, C-11, C-13), 123.19 (CH, C-18, C-20), 106.59 (CH, C-25, C-26), 13.54 (CH, C-28, C-29-diCH_3); MS (ESI): m/z = found 495.15 [M-2], 497.09 [M^+] (calcd. 497.37); anal. calcd. For $C_{22}H_{17}N_4O_3SBr$: C, 53.13; H, 3.45; N, 11.26; Found: C, 53.48; H, 3.76; N, 11.53.

N-[5-bromo-4-(4-methoxyphenyl)-1,3-thiazol-2-yl]-4-(2,5-dimethyl-1H-pyrrol-1-yl)benzamide (6e)

Compound **6e** was obtained as red solid (yield 90%). m.p. 178–180 °C; FTIR (KBr): 3307, 2927, 1668, 1609 cm^{-1}; ^1H NMR (400 MHz, DMSO-d_6) δ ppm: 10.74 (1H, s, NH), 8.00 (2H, d, $J = 2.2$ Hz, H-17, H-21), 7.84 (2H, d, $J = 3.4$ Hz, H-18, H-20), 7.67 (2H, d, $J = 2.0$ Hz, H-10, H-14), 7.35 (2H d, $J = 2.3$ Hz, H-11, H-13), 5.82 (2H, s, H-25, H-26), 3.80 (3 H, s, OCH_3), 2.00 (6H, s, H-28, H-29-diCH_3); ^{13}C NMR (75 MHz, DMSO-d_6) δ ppm: 168.19 (CO, C-8), 166.38 (C-2), 133.01 (C-4), 131.45 (C-16), 130.38 (C-12), 128.21 (C-9), 127.95 (C-19), 127.78 (CH, C-10, C-14), 127.25 (CH, C-17, C-21), 124.13 (CH, C-11, C-13), 123.25 (CH, C-18, C-20), 120.89 (CH, C-10, C-14), 108.88 (CH, C-25, C-26), 102.32 (C-5), 26.35 (C-22, OCH_3), 13.35 (C-28, C-29-diCH_3); MS (ESI): m/z = found 482.38 [M^+], 484.48 [M + 2] (calcd. 482.40); anal. calcd. For $C_{23}H_{20}N_3O_2SBr$: C, 57.27; H, 4.18; N, 8.71; Found: C, 57.57; H, 4.35; N, 8.92.

N-(5-bromo-4-phenyl-1,3-thiazol-2-yl)-4-(1H-pyrrol-1-yl) benzamide (7a)

Compound **7a** was obtained as Pale yellow solid (yield 82%). m.p. 178–180 °C; FTIR (KBr): 3290, 3137, 1681, 1608 cm^{-1}; ^1H NMR (400 MHz, DMSO-d_6) δ ppm: 13.07 (1H, s, NH), 8.25 (2H, d, $J = 3.2$ Hz, H-18, H-20), 8.01 (2H, d, $J = 8.5$ Hz, H-17, H-21), 7.82 (2H, d, $J = 8.1$ Hz, H-10, H-14), 7.66-7.21 (3H, m, H-11, H-12, H-13), 7.07 (2H, d, $J = 30.3$ Hz, H-23, H-26), 6.33 (2H, d, $J = 6.2$ Hz, H-24, H-25); ^{13}C NMR (75 MHz, DMSO-d_6) δ ppm: 168.19 (CO, C-8), 166.76 (C-5), 151.11 (C-4), 143.06 (C-16), 133.08 (C-12), 131.06 (C-9), 130.11 (C-19), 128.77 (C-10, C-14), 128.46 (CH, C-17, C-21), 127.09 CH, (C-11, C-13), 119.05 (CH, C-18, C-20), 118.58 (CH, C-23, C-26), 111.39 (C-24, C-25), 98.09 (C-5); MS (ESI): m/z = found 424.33 [M^+], 425.33 [M + 2] (calcd. 424.32); anal. calcd. For $C_{20}H_{14}N_3OSBr$: C, 56.61; H, 3.33; N, 9.90; Found: C, 56.63; H, 3.39; N, 9.99.

N-[5-bromo-4-(4-bromophenyl)-1,3-thiazol-2-yl]-4-(1H-pyrrol-1-yl)benzamide (7b)

Compound **7b** was obtained as pale yellow solid (yield 80%). m.p. 158–160 °C; FTIR (KBr): 3360, 3173, 1654, 1611 cm^{-1}. ^1H NMR (400 MHz, DMSO-d_6) δ ppm: 12.61 (1H, s, NH), 7.85 (2H, d, $J = 1.7$ Hz, H-17, H-21), 7.84 (2H, d, $J = 1.7$ Hz, H-18, H-20), 7.56 (2H, d, $J = 1.8$ Hz, H-10, H-14), 7.35 (2H, d, $J = 2.2$ Hz, H-11, H-13), 7.24 (2H, d, $J = 3.6$ Hz, H-24, H-27), 6.17 (2H, d, $J = 2.1$ Hz, H-25, H-26). ^{13}C NMR (75 MHz, DMSO-d_6) δ ppm: 167.07 (CO, C-8), 164.05 (C-2), 151.02 (C-4), 144.06 (C-16), 132.08 (C-12), 131.86 (C-9), 130.61 (C-19), 128.67 (C-10, C-14), 128.66 (CH, C-18, C-20), 126.89 (CH, C-11, C-13), 118.05 (C-18,C-20), 117.58 (CH, C-24,C-27), 110.39 (CH, C-25, C-26), 97.09 (C-5); MS (ESI): m/z = found 502.87 [M^+], 504.79 [M + 2], 506.09 [M + 4] (calcd. 503.21); anal. calcd. For $C_{20}H_{13}N_3OSBr_2$: C, 47.74; H, 2.60; N, 8.35; Found: C, 48.04; H, 2.70; N, 8.45.

Synthesis of 5-bromo-4-phenyl-2-(1H-pyrrol-1-yl) thiazole (8)

The 5-bromo-4-phenylthiazole (0.01 mol) and 2,5-dimethoxytetrahydrofuran (0.012 mol) were refluxed in dry acetic acid (15 mL) for 45 min, which was then poured into ice cold water with stirring to yield 5-bromo-4-phenyl-2-(1*H*-pyrrol-1-yl)thiazole (**8**) (Scheme 1).

5-bromo-4-phenyl-2-(1H-pyrrol-1-yl)-1,3-thiazole (8)

Compound **8** was obtained as white solid (yield 80%). m.p. 152–154 °C; FTIR (KBr): 3392, 2923, 1515 cm^{-1}; ^1H NMR (400 MHz, DMSO-d_6) δ ppm: 7.98–7.71 (3H, m, H-13, H-14, H-15), 7.52 (2H, d, $J = 3.6$ Hz, H-12, H-16), 7.32 (2H, d, $J = 6.8$ Hz, H-7, H-10), 7.26 (2H, d, $J = 4.4$ Hz, H-8, H-9); ^{13}C NMR (75 MHz, DMSO-d_6) δ ppm: 163.73 C-2), 162.25 (C-4), 135.83 (C-11), 129.90 (C-12), 128.12 (CH, C-13, C-15), 127.02 (CH, C-12, C-16), 123.99 (CH, C-7, C-10), 108.59 (CH, C-8, C-9), 95.94 (C-5); MS (ESI): m/z = found 307.14 [M + 2] (calcd. 305.19); anal. calcd. For $C_{13}H_9N_2SBr$: C, 51.16; H, 2.97; N, 9.18; Found: C, 51.39; H, 3.01; N, 9.36.

General procedure for the synthesis of *N*-benzyl-4-(2,5-dimethyl-1*H*-pyrrol-1-yl)benzamide (10)/4-(2,5-dimethyl-1*H*-pyrrol-1-yl)-*N*-(substituted phenyl) benzamides (11a–d)

Different aromatic amines (0.0018 mol) and 4-(2, 5-dimethyl-1*H*-pyrrol-1-yl)benzoic acid (**9b**) (0.0019 mol) were dissolved, respectively, in 50 mL of dry dimethyl formamide. HBTU (0.87 g, 0.0023 mol) and DIEA (0.93 mL, 0.0053 mol) were then added to the above mixture and stirred for 24–30 h at the ambient temperature. The reaction was quenched by adding NaCl solution and the mixture was extracted with ethyl acetate (3 × 50 mL). The combined ethyl acetate layer was washed with 1 N HCl and with the saturated sodium bicarbonate followed by NaCl solution. The organic layer was dried over an anhydrous sodium sulfate and concentrated using rotary flash evaporator. Thus obtained residue was dried and purified by column chromatography using petroleum ether:ethyl acetate (6:4) mixture as the eluent to afford the desired compounds (**10**) and (**11a–d**) (Scheme 2).

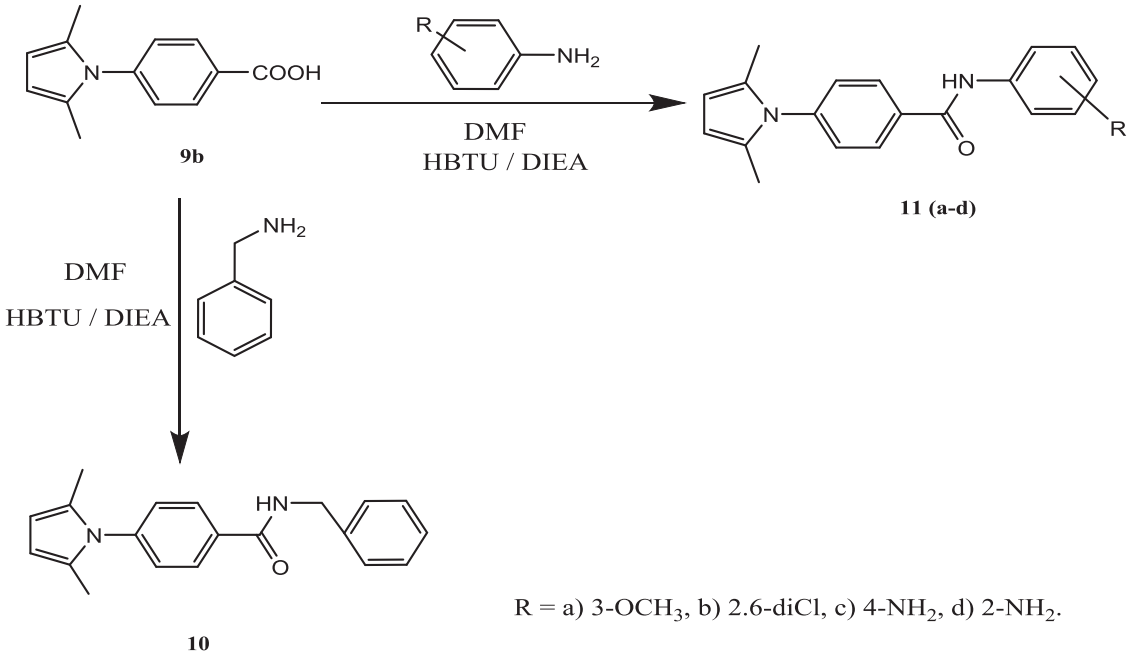

R = a) 3-OCH_3, b) 2.6-diCl, c) 4-NH_2, d) 2-NH_2.

Scheme. 2 Synthesis of substituted 2,5-dimethylpyrrolyl benzamides

N-benzyl-4-(2,5-dimethyl-1H-pyrrol-1-yl)benzamide (10)

Compound **10** was obtained as yellow solid (yield 90%). m.p. 158–160 °C; FTIR (KBr): 3299, 2921, 1635, 1607 cm^{-1}; ^1H NMR (400 MHz, DMSO-d_6) δ ppm: 9.18 (1H, s, NH), 8.03 (2H, d, $J = 8.4$ Hz, H-7, H-11), 7.39 (2H, d, $J = 8.4$ Hz, H-8, H-10), 7.34–7.25 (3H, m, H-20, H-21, H-22), 7.24 (2H, d, $J = 4.8$ Hz, H-19, H-23), 5.82 (2H, s, H-3, H-4), 4.52 (2 H, d, J = 6.0 Hz, CH_2), 1.98 (6H, s, H-12, H-13-diCH_3); ^{13}C NMR (75 MHz, DMSO-d_6) δ ppm: 166.15 (CO, C-15), 141.29 (C-6), 138.98 (C-18), 133.76 (C-9), 128.76 (CH, C-7, C-11), 128.29 (CH, C-19, C-23), 128.01 (CH, C-8, C-10), 127.67 (CH, C-20, C-22), 126.25 (C-21), 122.25 (CH, C-2, C-5), 106.87 (CH, C-3, C_4), 43.15 (C-17, CH_2), 13.32 (C-12, C-13, Pyrrole-diCH_3); MS (ESI): m/z = found 303.46 [M-1] (calcd. 304.39); anal. calcd. For $C_{20}H_{20}N_2O$: C, 78.92; H, 6.62; N, 9.20; Found: C, 79.04; H, 6.87; N, 9.44.

4-(2,5-dimethyl-1H-pyrrol-1-yl)-N-(3-methoxyphenyl) benzamide (11a)

Compound **11a** was obtained as light yellow solid (yield 80%). m.p. 106–108 °C; FTIR (KBr): 3291, 2918, 1642, 1608 cm^{-1}; ^1H NMR (400 MHz, DMSO-d_6) δ ppm: 10.35 (1H. s, NH), 8.07 (2H, d, $J = 8.4$ Hz, H-7, H-11), 7.50–7.28 (3H, m, H-20, H-21, H-22), 7.26 (2H, d, $J = 8.0$ Hz, H-8, H-10), 6.71 (1H, s, H-18), 5.84 (2H, s, H-3, H-4), 3.76 (3H, s, –OCH_3), 2.01 (6H, s, H-12, H-13-diCH_3). ^{13}C NMR (75 MHz, DMSO-d_6) δ ppm: 165.44 (CO, C-15), 141.51 (C-6), 134.48 (C-17), 129.64 (C-9), 129.19 (CH, C-7, C-11), 128.33 (CH, C-18, C-22), 128.03 (CH, C-8, C-10), 123.01 CH, (C-19, C-21), 121.36 (C-20), 109.66 (CH, C-2, C-5), 106.94 (CH, C-3, C-4), 55.47 (C-19, OCH_3), 13.39 (C-12, C-13-diCH_3); MS (ESI): m/z = found: 321.06 [M + H] (calcd. 320.39); anal. calcd. For $C_{20}H_{20}N_2O_2$: C, 74.98; H, 6.29; N, 8.74; Found: C, 75.08; H, 6.41; N, 8.89.

N-(2,6-dichlorophenyl)-4-(2,5-dimethyl-1H-pyrrol-1-yl) benzamide (11b)

Compound **11b** was obtained as light yellow solid (yield 72%). m.p. 104–106 °C; FTIR (KBr): 3381, 2922, 1696, 1604 cm^{-1}; ^1H NMR (400 MHz, DMSO-d_6) δ ppm: 13.22 (1H. s, NH), 8.16 (2H, d, $J = 40.0$ Hz, H-1, H-11), 7.76 (2H, d, $J = 4.0$ Hz, H-8,H-10), 7.41–7.30 (3H, m, H-19, H-20, H-21), 5.83 (2H, s, H-3, H-4), 1.99 (6H, s, H-12, H-13-diCH_3); ^{13}C NMR (75 MHz, DMSO-d_6) δ ppm: 167.36 (CO, C-8), 142.48 (C-6), 130.76 (C-17), 128.42 (C-9), 128.00 (CH, C-7, C-11), 127.38 (CH, C-18, C-22), 126.91 (CH,C-8, C-10), 125.16 (CH, C-19, C-21), 124.26 (C-20), 111.91 (CH, C-2, C-5), 106.61 (CH, C-3, C-4), 20.80, 13.30 (C-12, C-13-diCH_3); MS (ESI): m/z = found: 359.27 [M^+], 361.15 [M + 2] (calcd. 359.25); anal. calcd. For $C_{19}H_{16}N_2OCl_2$: C, 63.52; H, 4.49; N, 7.80; Found: C, 63.65; H, 4.62; N, 8.01.

N-(4-aminophenyl)-4-(2,5-dimethyl-1H-pyrrol-1-yl) benzamide (11c)

Compound **11c** was obtained as light yellow solid (yield 85%). m.p. 124–126 °C; FTIR (KBr): 3924, 2920, 1646,

1607 cm^{-1}; ^1H NMR (400 MHz, DMSO-d_6) δ ppm: 10.00 (1H, s, NH), 8.09 (2H, d, $J = 8.4$ Hz, H-7, H-11), 8.06 (2H, d, $J = 12.0$ Hz, H-8, H-10), 7.46 (2H, d, $J = 6.4$ Hz, H-19, H-21), 7.41 (2H, d, $J = 2.8$ Hz, H-18, H-22), 5.85 (2H, d, $J = 5.6$ Hz, H-3, H-4), 4.95 (2H, s, NH_2), 2.00 (6H, s, H-12, H-13-diCH_3); ^{13}C NMR (75 MHz, DMSO-d_6) δ ppm: 165.30 (CO, C-8), 145.73 (C-6), 141.48 (C-17), 134.42 (C-9), 129.48 (CH, C-7, C-11), 129.18 (CH, C-18, C-22), 128.96 (CH, C-8, C-10), 128.23 (CH, C-19, C-21), 120.96 (C-20), 113.13 (CH, C-2, C-5), 106.89 (CH, C-3, C-4), 29.36, 13.36 (C-12, C-13-diCH_3); MS (ESI): m/z = found: 305.42 [M^+] (calcd. (305.38); anal. calcd. For $C_{19}H_{19}N_3O$: C, 74.73; H, 6.27; N, 13.76; Found: C, 74.93; H, 6.47; N, 13.92.

N-(2-aminophenyl)-4-(2,5-dimethyl-1H-pyrrol-1-yl) benzamide (11d)

Compound **11d** was obtained as light yellow solid (yield 85%). m.p. 134–136 °C; FTIR (KBr): 3223, 2972, 1647, 1608 cm^{-1}; ^1H NMR (400 MHz, DMSO-d_6) δ ppm: 9.77 (1H, s, NH), 8.12 (2H, d, $J = 8.0$ Hz, H-7, H-11), 7.70 (2H, d, $J = 3.2$ Hz, H-8, H-10), 7.69–7.30 (4H, m, H-19, H-20, H-21), 7.18 (1H, d, $J = 7.6$ Hz, H-22), 5.84 (2H, s, H-3, H-4), 4.95 (2H, s, -NH_2), 2.01 (6H, s, H-12, H-13-diCH_3); ^{13}C NMR (75 MHz, DMSO-d_6) δ ppm: 165.13 (CO, C-15), 143.78 (C-6), 141.37 (C-17), 134.13 (C-20), 128.46 (CH, C-7, C-11), 128.23 (CH, C-18, C-22), 128.02 (CH, C-8, C-10), 127.31 (CH, C-19, C-21), 127.09 (C-20), 116.52 (CH, C-2, C-5), 106.90 (CH, C-3, C-4), 13.40 (CH, C-12, C-13-diCH_3); MS (ESI): m/z = found: 305.19 [M^+] (calcd. 305.38); anal. calcd. For $C_{19}H_{19}N_3O$: C, 74.73; H, 6.27; N, 13.76; Found: C, 74.90; H, 6.44; N, 13.98.

Biological activity

In vitro evaluation of antitubercular studies

All the compounds were tested for inhibition of *M. tuberculosis* strain $H_{37}Rv$ using the Microplate Alamar Blue Assay (MABA) method described earlier (Franzblau et al. 1998). The 96 wells plate received 100 mL of Middlebrook 7H9 broth and serial dilution of compounds were made directly on the plate with drug concentrations of 0.2, 0.4, 0.8, 1.6, 3.125, 6.25,12.5, 25, 50, and 100 µg/mL. Plates were covered and sealed with parafilm and incubated at 37 °C for 5 days. Then, 25 mL of freshly prepared 1:1 mixture of alamar blue reagent and 10% Tween 80 were added to the plate and incubated for 24 h. A blue color in the well was interpreted as no bacterial growth, while the appearance of pink color was scored as the growth. The MIC value (defined as the lowest drug concentration) prevented the color change from blue to pink. Table 1 shows the anti-TB activity data expressed in MIC.

Table 1 In vitro evaluation of antitubercular activity (MIC values in µg/mL) and enzyme inhibition values (results are expressed as % InhA inhibition)

Comp.	MIC values (µg/mL) (*M. tuberculosis* H37Rv)	% Inhibition at 50 µM
3a	25	NI[a]
3b*	1.6	25
3c	3.12	NT[b]
3d*	1.6	30
3e*	1.6	NT[b]
4a	50	NT[b]
4b	1.6	NT[b]
4c	1.6	38
4d	12.5	NT[b]
4e	1.6	38
4f	1.6	NT[b]
6a	12.5	NT[b]
6b*	1.6	NT[b]
6c*	1.6	NT[b]
6d	3.12	NT[b]
6e*	1.6	NT
7a	12.5	NT[b]
7b	6.25	NT[b]
8	1.6	NT[b]
10	3.12	12
11a	12.5	NT[b]
11b	1.6	31
11c	1.6	30
11d	3.12	12
Pyrazinamide	3.12	–
Streptomycin	6.25	–
Triclosan	–	>99

Astrisk indicates the compounds used for Pharmacophore mapping

[a]NI stands for no inhibition

[b]NT stands for not tested

In vitro evaluation of antibacterial activity

MIC determination of the tested compounds was investigated side-by-side by comparison with ciprofloxacin against Gram-positive (*S. aureus*) and Gram-negative bacteria (*E. coli*) using the broth microdilution method (Goto et al. 1981; Villanova 1985). Serial dilutions of the test compounds and reference drugs were done in Mueller–Hinton agar. Drugs (10 mg) were dissolved in dimethylsulfoxide (DMSO, 1 mL). Further progressive dilutions with the molten Mueller–Hinton agar were performed to obtain the required concentrations of 0.2, 0.4, 0.8, 1.6, 3.125, 6.25,

12.5, 25, 50, and 100 µg/mL. The tubes were then inoculated with 10^5 cfu/mL (colony forming unit/mL) and incubated at 37 °C for 18 h. MIC represents the lowest concentration of the tested compound that yielded no visible growth on the plate. To ensure that solvent did not affect bacterial growth the control experiment was performed with the test medium supplemented with DMSO using the same dilutions as used for the molecules in the experiment, but DMSO did not show any effect on the microorganisms in the studied concentration range. Table 2 summarizes the antibacterial activity data expressed in MIC values.

Table 2 In vitro evaluation of antibacterial activity (MIC values in µg/mL) and MTT-based cytotoxicity activity of selected compounds against human lung cancer cell lines A549 and MV cell line (IC_{50} in µg/mL)

Compound	IC_{50} (µM)[a]		Gram negative	Gram positive
	MV cell-lines[b]	A_{549}[c]	*E. coli* (µg/mL)	*S. aureus* (µg/mL)
3a	–	–	25	25
3b	220 ± 0.8	218 ± 0.7	25	3.12
3c	–	–	50	6.25
3d	212 ± 0.6	216 ± 0.2	12.5	3.12
3e	–	–	12.5	3.12
4a	–	–	50	25
4b	–	–	25	3.12
4c	214 ± 0.2	216 ± 0.5	25	1.6
4d	–	–	25	6.25
4e	217 ± 0.3	214 ± 0.4	25	1.6
4f	–	–	25	1.6
6a	–	–	50	6.25
6b	–	–	12.5	1.6
6c	–	–	12.5	3.12
6d	–	–	25	3.12
6e	–	–	25	3.12
7a	–	–	50	12.5
7b	–	–	50	6.25
8	–	–	50	3.12
10	218 ± 0.3	216 ± 0.4	50	12.5
11a	–	–	50	3.12
11b	210 ± 0.3	214 ± 0.4	50	3.12
11c	216 ± 0.4	216 ± 0.7	25	3.12
11d	219 ± 0.2	211 ± 0.3	25	6.25
Ciprofloxacin	–		2	2
INH	>450	>450		

[a]Cytotoxicity is expressed as IC_{50} which is the concentration of compound reducing by 50% of the optical density of treated cells with respect to untreated cells using MTT assay. Values are the means ± SEM of three independent experiments

[b]Mammalian Vero cell-lines (NCCS-Pune, India)

[c]A549 (lung adenocarcinoma) cell-lines (NCCS-Pune, India)

MTT-based cytotoxicity activity

Cellular conversion of MTT [3-(4,5-dimethylthiazo-2-yl)-2,5-diphenyl-tetrazolium bromide] into a formazan product (Mosmann 1983) was performed to evaluate cytotoxic activity (IC_{50}) of some of the compounds against A549 (lung adenocarcinoma) MV cell-lines up to concentration of 50 mg/mL using Promega Cell Titer 96 non-radioactive cell proliferation assay (Gundersen et al. 2002) using cisplatin as the positive control. The IC_{50} values given in Table 2 are the averages ± SEM of three independent measurements.

Enzyme inhibition studies

InhA expression and purification

The production and purification of InHA-6xHis protein from a protease-deficient strain of *E. coli* (BL21) transformed with pHAT5/InhA plasmid were performed. A 1 mL of bacteria was grown in 100 mL of Lysogeny broth (LB) medium containing ampicillin (100 µg/mL) and 2% glucose at 37 °C. After 4 h, the solution was re-diluted in 1 L of the same medium and re-grown at 37 °C. After attaining proper concentration ($OD_{595} = 0.6–0.8$), the culture was centrifuged at 3300 g factor for 10 min at 4 °C and bacteria were suspended in LB medium containing ampicillin (100 µg/mL). Protein expression was induced for overnight incubation in 1 mM isopropyl-β-D-galactopyranoside (IPTG) at 20 °C. Cells were harvested by centrifugation at 6000×*g* for 30 min at 4 °C. Dry pellet was kept at −80 °C for several months and purification was done with Ni-NTA Agarose from QIAGEN following the manufacturer's protocol. The purified recombinant protein was applied to PD-10 desalting columns (GE Healthcare, Piscataway, NJ) equilibrated with PIPES 30 mM pH 6.8 and 150 mM NaCl to remove the imidazole. Samples were analyzed using SDS–PAGE and Coomassie blue staining and then stored at 4 °C for a short-time at −80 °C with 20% glycerin for long-term storage (Menendez et al. 2011).

InhA activity inhibition

Triclosan and NADH were obtained from Sigma-Aldrich (Bangalore, INDIA). Stock solutions of the selected compounds were prepared in DMSO such that the final concentration of this co-solvent was constant at 5% (v/v) in the final volume of 1 mL for all the kinetic reactions. Kinetic assays were performed using *trans*-2-dodecenoyl-coenzyme A (DDCoA) and wild type InhA as previously described (Menendez et al. 2012). Briefly, the reactions were performed at 25 °C in an aqueous buffer (30 mM PIPES and 150 mM NaCl, pH 6.8) containing 250 µM cofactor (NADH), 50 µM substrate (DDCoA) and the test compound (at 50 µM).

Reactions were initiated by adding InhA (100 nM final) and NADH oxidation was monitored at the fixed wavelength of 340 nm. Inhibitory activity of each derivative was expressed as % inhibition of InhA activity (initial velocity of the reaction) with respect to control reaction without the inhibitor. These results are shown in Table 1.

Computational details

General method

The crystal structure of enoyl acyl carrier protein reductase InhA in complex with *N*-(4-methylbenzoyl)-4-benzylpiperidine (PDB ID 2NSD, 1.9 Å X-ray resolution) was retrieved from the Brookhaven Protein Database (PDB http://www.rcsb.org/pdb). In the current condition, biopolymer and each molecule in the data set were energetically minimized by employing the Tripos force field (Clark et al. 1989). Powell optimization method (Powell 1977), Amber7FF9902 (biopolymer) and MMFF94 (molecules) charges (NB cut-off 9.0 as well as dielectric constant 4.0) with a convergence criterion set at 0.001 kcal/mol Å. The pharmacophore models were generated and analyzed using GALAHAD (Genetic Algorithm with Linear Assignment of Hypermolecular Alignment of Datasets) module. All calculations were performed on a commercially available SYBYL-X 2.0 software package (Tripos Associates, St. Louis, MO, USA) (Tripose, USA 2012).

Docking protein–ligand interactions is a significant approach in current drug discovery research. If the composition of binding site is identified, subsequently modeling procedures will afford important insights into such interactions and in several affirmative cases, one can validate the hits from the virtual screening. In this process, pharmacophore-based 3D searching also proved to be beneficial (Guner, CA 2000). It is categorized in terms of subgroups of two, three or four features, and the preparation with particular characteristics, which are essential for molecule binding in addition to spatial connection among them gives a fast and flexible tool to perform these searches. The GALAHAD (Richmond et al. 2006) fit implemented in SYBYL 2.0 program was also employed in the building of pharmacophore hypothesis for the synthesized compounds, It is a distinctive technique, since it does not require any template structure, but allows for instant and efficient creation of partial-coverage models with multiple partial match constraints (Shepphird and Clark 2006).

Alignment and pharmacophore generation

In this study, a sum of 24 phenyl thiazole and pyrrolyl benzamide antimycobacterial molecules were used as data set to carry out pharmacophore hypothesis and modeling studies. All the ligands were aligned in two steps. In the first step, six compounds (**3b**, **3d**, **3e**, **6b**, **6c**, and **6e** labeled with asterisks shown in Table 1) were chosen to perform the pharmacophore hypothesis; the genetic algorithm was used to create the conformers for all the compounds. The molecules that were selected to create pharmacophore hypothesis were found to be exceptionally active. GALAHAD module was used for flexible alignment of all the selected ligands that are completely independent of template with a population size of 45 and a maximum generation value of 50 with molecules requiring hitting of 4. Twenty pharmacophore models were generated and analyzed on the basis of fitness scores and percentage of aligned molecule (Tripose, MO 2014). The experimentally obtained anti-TB activity of each molecule was denoted as minimal inhibitory concentration (MIC) against *M. tuberculosis* and MIC values were used in pharmacophore analysis.

GALAHAD formed a set of likely hypotheses by means of the flexible alignment (Table 3, 20 models). SPECIFICITY is a logarithmic indicator of the expected discrimination for each query. The actual number of hits is given in N_HITS column and the values in FEATS column indicate the total number of features in the model query. The next five columns are model score components from the genetic algorithm. Pareto is a Pareto rank of each model, where all the models have a Pareto rank of zero. This means none of the models are superior to any other when using all the four criteria in columns 5–8 (ENERGY, STERICS, H_BOND, and MOL_QRY). ENERGY calculated is the total energy of the model; STERICS is a steric overlap for the model; H_BOND, pharmacophoric concordance and MOL_QRY are in agreement between the query tuplet and pharmacophoric tuplets for ligands as a group. Last four columns are the scores for individual ligands within each model. Thus, in this case, every cell in each of the last four columns contains a list of five values.

For rigid alignment of the left over ligands in a data set (in the second step), we need to choose one best template model and choice of the model from the obtained 20 models in the first stage based on the model needed to “hit” all the six active compounds. The model required to have high sterics with low energy and pharmacophoric features. We have constructed the scatter plot (ENERGY vs. STERICS vs. MOL_QRY) to visualize the Pareto surface and selected the best pharmacophore model (Fig. 4). Taking into account the ENERGY, STERICS, and MOL_QRY criteria, the best model is depicted in the graph, where ENERGY is rationally low and STERICS score is high. Among the measured models, MODEL_18 (denoted with a black circle in Fig. 4) has the best position as it fulfills all the three criteria and has improved Specificity, N hits and Feats values (Caballero 2010; Zhao et al. 2010).

At the end, all the molecules were aligned with the use of pharmacophore (MODEL_18) as a template using GALAHAD's template procedure (Table 4). Pharmacophore and steric bitmaps were formed for each molecule and (compressed) the count vectors were then created for the band. Subsequently, the post-processing action in GALAHAD involves taking the genetic algorithm results and producing the final models together with their alignments, scoring of the models, and displaying their rank. In GALAHAD, the needed frame of reference is generated via post processing using hypermolecular alignment program linear assignment for molecular dataset alignment (LAMDA) (Tripose, MO 2014).

Surflex-docking

To generate and score the putative protein–ligand complexes according to their calculated binding affinities at the active site of ENR with ligands, molecular modeling was carried out using the Surflex-dock module of one more superior version of SYBYL software (X 2.0). Such docking approach aligns the ligand to a "protomol" also idealized ligand in the active site of the target. Surflex-Dock, which uses observed scoring function and a patented search engine (Jain 1996, 2003) was engaged for molecular modeling of the training set in addition to the test set compounds into the active site of the crystal structure of ENR catalytic core.

Results and discussion

Chemistry

All the reactions were carried out as per Schemes 1 and 2. The *Pall–Knorr* pyrrole synthesis involves the reaction of amine with diketone viz., 2,5-dimethoxytetrahydrofuran/2,5-hexane dione, which is the general method for the synthesis of pyrrole ring as used for compounds (**3a–e**), (**4a–f**), (**6a–e**), (**7a,b**), **8**, **9**, **10** and (**11a–d**).

In Scheme 1, 2-amino-4-(substituted phenyl)thiazoles (**2a–f**) were synthesized as described earlier in which 4-substituted acetophenones (**1a–f**) were used as the starting materials.

The reaction of 2-amino-4-(4-substituted phenyl)thiazoles **(2a–f)** with 4-(1*H*-pyrrolyl-1-yl)benzoic acid/4-(2,5-dimethyl-1*H*-pyrrolyl-1-yl)benzoic acid, respectively using HBTU as a coupling agent and DIEA as a base in DMF medium to give *N*-4-(4-substituted phenyl)thiazole-2-yl-4-(1*H*-pyrrol-1yl)bezamides (**3a–e**)/*N*-4-(4-substituted phenyl)thiazol-2-yl-4-(2,5-dimethyl-1*H*-pyrrol-1-yl)benzamides (**4a–f**). The reaction of 4-(4-substituted phenyl)-5-bromo-2-aminothiazoles (**5a–e**) with 4-(2, 5-dimethyl-1

Table 3 Different pharmacophore models using GALAHAD

	Specificity	N_Hits	FEATS	PARETO	ENERGY	STERICS	H_BOND	MOL_QRY
Model_01	5.875	6	8	0	0.78	1727.10	54.30	37.44
Model_02	4.452	6	8	0	41.73	1952.00	54.20	35.50
Model_03	4.455	6	8	0	37.69	1988.50	54.60	32.57
Model_04	4.444	6	8	0	47.61	1937.50	54.30	36.33
Model_05	4.450	6	8	0	44.76	2050.80	52.70	37.31
Model_06	4.446	6	8	0	54.09	1884.50	54.10	38.21
Model_07	4.451	6	8	0	54.00	1694.10	55.50	39.01
Model_08	4.449	6	8	0	53.95	1743.20	55.50	35.65
Model_09	4.458	6	8	0	27.57	1865.60	54.10	28.05
Model_10	4.681	7	8	0	41.04	1818.60	53.60	37.00
Model_11	4.445	6	8	0	20.89	1863.30	51.40	34.38
Model_12	4.454	6	8	0	20.52	1785.50	52.40	33.79
Model_13	4.452	13	8	0	1659.19	1748.60	55.50	38.52
Model_14	4.449	13	8	0	17.33	1889.00	51.50	26.35
Model_15	4.335	4	11	0	27.04	1520.80	53.70	39.15
Model_16	4.452	6	8	0	84.26	2009.90	54.20	31.85
Model_17	3.698	6	7	0	31.63	1401.40	54.80	34.78
Model_18	**4.169**	**7**	**9**	**0**	**60.41**	**2087.40**	**54.30**	**23.33**
Model_19	5.888	13	8	0	91.18	2037.50	54.70	26.07
Model_20	3.002	6	11	0	40.42	1808.60	52.50	35.51

Table 3 (continued)

IND_ENERGY							
Model_01	24.60 11.84	3.26 35.47	16.55 65.76	34.84 0.24	13.01 24.43	11.00 16.70	12.47
Model_02	19.00 16.15	75.79 59.68	9.11 107.11	45.51 11.42	53.79 22.85	16.62 15.10	90.39
Model_03	17.09 13.74	146.02 46.03	8.32 27.50	51.10 0.94	15.69 25.40	32.76 15.18	90.26
Model_04	17.06 14.79	187.06 9.73	22.20 15.44	22.76 3.13	73.98 25.03	192.25 21.90	13.66
Model_05	93.32 18.26	9.51 18.14	125.47 18.09	54.94 0.16	11.86 16.03	121.56 15.17	79.34
Model_06	25.06 16.13	75.75 181.36	9.77 103.11	48.02 62.33	51.06 22.17	11.30 15.10	82.02
Model_07	24.01 10.34	9.22 20.56	59.15 44.96	31.80 0.72	14.93 25.53	424.49 17.41	18.84
Model_08	11.30 15.34	56.77 20.01	53.99 46.29	27.30 0.72	50.99 24.81	201.86 17.55	174.48
Model_09	16.48 16.06	87.84 44.79	10.06 27.47	74.81 -0.29	14.58 17.74	27.17 16.13	5.60
Model_10	135.81 78.02	91.73 -1.16	15.15 55.21	6.12 13.63	17.22 32.19	14.65 18.08	56.94
Model_11	3.47 36.88	12.91 0.79	15.47 37.85	61.74 16.42	17.33 25.17	19.41 16.08	7.99
Model_12	23.35 20.44	14.75 0.72	15.35 51.04	4.62 13.99	15.54 25.25	5.74 17.43	58.47
Model_13	31.49 40.79	155.79 3.29	47.97 69.45	20747.56 15.79	177.20 22.81	158.89 16.10	82.38
Model_14	19.60 20.44	11.56 −0.59	22.37 28.32	11.54 15.19	13.27 20.45	36.48 17.49	9.11
Model_15	29.22 66.75	9.53 −0.12	30.04 16.15	27.97 14.63	74. 0420.29	15.67 16.51	30.82
Model_16	150.92 37.34	191.38 −0.49	412.51 39.89	17.19 10.34	31.31 21.55	15.89 16.63	150.98
Model_17	13.67 48.70	28.97 5.97	50.91 17.98	6.19 16.42	83.06 21.96	83.71 16.20	17.42
Model_18	**150.25 68.53**	**182.48 −0.49**	**47.26 60.99**	**12.77 16.84**	**7.99 20.91**	**77.12 16.63**	**124.00**
Model_19	150.25 91.29	182.49 −0.49	415.73 58.57	8.56 18.26	11.46 20.12	35.01 16.72	177.31
Model_20	164.68 109.44	5.92 −0.12	16.09 26.06	12.83 16.45	87.00 21.49	20.30 16.22	29.13
IND_STERICS							
Model_01	125728.00 116054.34	113143.00 2005.33	125245.00 69088.66	119119.34 89306.66	147171.50 123132.66	155602.50 115265.30	63565.00
Model_02	141064.00 166537.83	148928.83 2941.17	128222.00 66178.50	132405.17 126074.50	167330.50 147475.33	133493.83 125793.66	59248.50
Model_03	139829.50 186882.50	149756.17 2631.83	104814.84 63858.67	122785.66 124120.00	176841.67 154035.67	190148.00 130358.66	63632.17
Model_04	153554.67 151482.00	161768.00 2845.17	134203.50 67292.34	137249.67 133986.83	176332.50 138944.33	182631.33 84494.34	53758.67
Model_05	118006.66 181677.00	143312.83 2269.00	124511.50 56277.83	124740.84 154460.17	183383.17 171050.67	186935.33 156661.67	49913.00
Model_06	147265.17 163653.33	154093.33 2889.17	138497.83 60888.83	135441.50 125500.84	154179.67 137906.17	114091.16 120633.66	55533.67
Model_07	138198.00 131826.00	143795.67 2323.33	104401.50 66739.84	85780.50 86346.66	135624.83 115213.84	142190.67 112389.34	57773.17
Model_08	134590.83 132310.67	147462.50 2296.67	121397.66 56486.67	122357.84 85299.66	143712.00 119304.00	136449.33 114769.00	50935.00
Model_09	145769.33 144733.67	154769.83 2743.17	104354.50 64527.17	119482.34 102169.00	160062.17 112719.84	164857.33 102571.50	60414.17
Model_10	141280.50 123114.66	154185.67 2211.50	136699.33 61425.83	135786.33 112506.66	126675.16 118553.66	121075.66 106312.66	58148.83
Model_11	121903.66 135301.83	142349.00 3050.33	131044.66 59946.67	128552.00 104095.34	167723.83 139038.00	158654.50 135410.33	54812.83
Model_12	155825.00 125182.84	162767.50 2336.17	131800.83 73321.66	129568.34 91335.00	140012.00 114313.00	135675.83 101446.84	66325.50
Model_13	119612.16 149939.17	117106.16 2911.50	112882.84 62547.67	106544.84 126067.50	156905.33 103460.16	125541.00 120613.84	56854.67
Model_14	139555.33 151183.17	150275.33 2803.00	128190.34 54637.00	130310.84 110984.00	159472.67 143341.67	119661.50 135012.33	49620.17
Model_15	110655.84 105439.66	126202.34 2330.50	122009.16 47194.50	120528.66 81139.00	92886.50 83345.66	93762.00 86932.50	40603.50
Model_16	128391.66 181807.00	134010.33 1803.83	105237.66 69386.16	116695.84 145834.83	198011.67 162995.17	192417.67 144924.83	61225.33
Model_17	115155.34 106945.16	116534.50 2876.50	114664.16 56156.17	112407.00 77757.66	83944.16 75455.00	102019.66 83744.34	53558.00
Model_18	**152415.50 178056.00**	**157141.17 1768.83**	**134237.50 62502.50**	**130606.34 124857.16**	**185413.17 151342.00**	**172858.00 140508.00**	**59432.50**
Model_19	146433.00 174355.00	154944.00 1656.50	104062.50 68652.34	119715.66 148939.83	173709.67 162659.83	163321.00 147774.00	60880.33
Model_20	131733.00 120048.50	143763.83 2317.83	98387.66 66906.66	118147.34 96074.84	150328.33 138679.17	144201.00 130016.50	59407.83
IND_HBOND							
Model_01	3506.33 6932.67	4028.00 141.33	4028.00 1950.00	4028.00 5873.67	5998.67 6932.67	5505.33 6778.67	1860.00

Table 3 (continued)

IND_ENERGY							
Model_02	4277.67 6795.67	4277.67 374.00	4277. 67 1950.00	4277.67 5898.33	5898.33 6795.67	4755.00 6612.33	1860.00
Model_03	3891.33 6741.00	3891.33 190.33	3891.33 1950.00	3891.33 5843.67	5843.67 6741.00	5350.33 6557.67	1860.00
Model_04	3602.00 6908.33	3602.00 153.00	3863.67 1950.00	3863.67 5974.33	5974.33 6908.33	5481.00 6754.33	1860.00
Model_05	3948.67 6627.33	3948.67 153.00	3530.00 1950.00	3948.67 5816.67	5816.67 6627.33	4699.33 6374.67	1860.00
Model_06	3506.33 6896.00	4028.00 141.33	4028.00 1950.00	4028.00 5998.67	5998.67 6896.00	5380.33 6712.67	1860.00
Model_07	4235.67 7021.33	4235.67 132.00	4235.67 1950.00	4235.67 5962.33	6087.33 7021.33	5594.00 6867.33	1860.00
Model_08	4235.67 7021.33	4235.67 132.00	4235.67 1950.00	4235.67 5962.33	6087.33 7021.33	5594.00 6867.33	1860.00
Model_09	4066.00 6889.00	4066.00 332.00	4066.00 1950.00	3497.00 5931.67	5991.67 6829.00	5498.33 6705.67	1860.00
Model_10	3725.67 6703.33	3723.33 169.33	3723.33 1950.00	3723.33 5769.33	5769.33 6703.33	5276.00 6549.33	1860.00
Model_11	3948.67 5827.67	3948.67 153.00	3530.00 1936.67	3948.67 5362.67	5487.67 6408.33	4398.33 6267.67	1860.00
Model_12	4028.00 6610.00	4028.00 141.33	3506.33 1950.00	4028.00 5587.67	5712.67 6610.00	4569.33 6426.67	1860.00
Model_13	4277.67 7026.67	4277.67 374.00	4277.67 1950.00	4277.67 6129.33	6129.33 7026.67	5511.00 6843.33	1860.00
Model_14	3792.33 6238.33	3792.33 204.00	3635.67 1950.00	3792.33 5367.67	5427.67 6238.33	4701.00 5812.33	1860.00
Model_15	3863.67 6816.67	3863.67 153.00	3602.00 1950.00	3602.00 5794.33	5919.33 6816.67	5426.00 6633.33	1860.00
Model_16	3723.33 6838.33	3725.67 169.33	3723.33 1950.00	3723.33 5904.33	5904.33 6838.33	5411. 00 6684.33	1860.00
Model_17	3850.00 6859.33	3850.00 153.00	4083.67 1950.00	4083.67 5837.00	5962.00 6859.33	5468.67 6676.00	1860.00
Model_18	**3863.67 6908.33**	**3863.67 153.00**	**3602.00 1950.00**	**3602.00 5974.33**	**5974.33 6908.33**	**5481.00 6754.33**	**1860.00**
Model_19	4028.00 6987.67	4028.00 141.33	3506.33 1950.00	4028.00 6053.67	6053.67 6987.67	5560.33 6833.67	1860.00
Model_20	3793.67 6042.33	3793.67 169.33	3633.33 1936.67	3633.33 5566.67	5691.67 6575.67	5198.33 6405.67	1860.00
IND_MOL_QRY							
Model_01	−4.30 −2.00	−4.10 −5.10	−4.10 −4.20	−4.10 −2.10	−2.00 −2.00	−2.40 −2.00	−4.20
Model_02	−4.20 −2.10	−4.20 −5.10	−4.20 −4.30	−4.20 −2.10	−2.10 −2.10	−2.90 −2.10	−4.30
Model_03	−4.50 −4.50	−4.50 −5.10	−4.50 −2.40	−4.50 −2.40	−2.40 −2.40	−2.70 −2.40	−4.50
Model_04	−4.10 −1.90	−4.10 −4.90	−3.90 −4.10	−3.90 −1.90	−1.90 −1.90	−2.30 −1.90	−4.10
Model_05	−3.90 −1.70	−3.90 −5.00	−4.10 −4.10	−3.90 −1.70	−1.70 −1.70	−2.60 −1.70	−4.10
Model_06	−3.90 −1.60	−3.70 −4.80	−3.70 −3.90	−3.70 −1.60	−1.60 −1.60	−2.00 −1.60	−3.90
Model_07	−3.90 −1.70	−3.90 −5.00	−3.90 −4.20	−3.90 −1.80	−1.70 −1.70	−2.00 −1.70	−4.20
Model_08	−4.20 −2.30	−4.20 −2.20	−4.20 −5.00	−4.20 −4.40	−2.20 −2.20	−2.50 −2.20	−4.40
Model_09	−4.40 −2.80	−4.40 −5.10	−4.40 −4.60	−4.20 −2.90	−2.80 −2.90	−3.00 −2.80	−4.60
Model_10	−3.80 −1.60	−4.00 −4.80	−4.00 −3.90	−4.00 −1.60	−1.70 −1.70	−2.20 −1.60	−3.90
Model_11	−4.10 −1.70	−4.10 −5.00	−4.00 −4.20	−4.10 −2.10	−2.00 −2.00	−2.90 −2.00	−4.20
Model_12	−4.30 −2.30	−4.30 −5.10	−4.20 −4.50	−4.30 −2.40	−2.30 −2.30	−3.00 −2.30	−4.50
Model_13	−3.90 −1.80	−3.90 −4.80	−3.90 −4.20	−3.90 −1.80	−1.80 −1.80	−2.00 −1.80	−4.20
Model_14	−4.80 −2.60	−4.80 −5.00	−4.60 −4.70	−4.80 −2.70	−2.60 −2.60	−3.50 −3.10	−4.70
Model_15	−12.70 −11.70	−12.70 −14.70	−12.90 −14.20	−12.90 −11.80	−11.70 −11.70	−11.90 −11.60	−14.20
Model_16	−4.40 −2.70	−4.50 −5.10	−4.40 −4.70	−4.40 −2.70	−2.70 −2.70	−3.00 −2.70	−4.70
Model_17	−3.00 −0.10	−2.80 −3.40	−3.00 −3.10	−2.80 −0.20	−0.10 −0.10	−0.60 −0.10	−3.10
Model_18	**−7.50 −5.90**	**−7.50 −8.00**	**−7.70 −7.70**	**−7.70 −5.90**	**−5.90 −5.90**	**−6.30 −5.90**	**−7.70**
Model_19	−5.00 −3.10	−5.00 −5.10	−5.00 −4.80	−5.00 −3.10	−3.10 −3.10	−3.60 −3.10	−4.80
Model_20	−13.10 −12.60	−13.10 −14.90	−13.30 −14.20	−13.30 −12.20	−12.10 −12.10	−11.80 −12.00	−14.20

MODEL_18 given in bold was considered for the final rigid alignment of the remaining compounds.

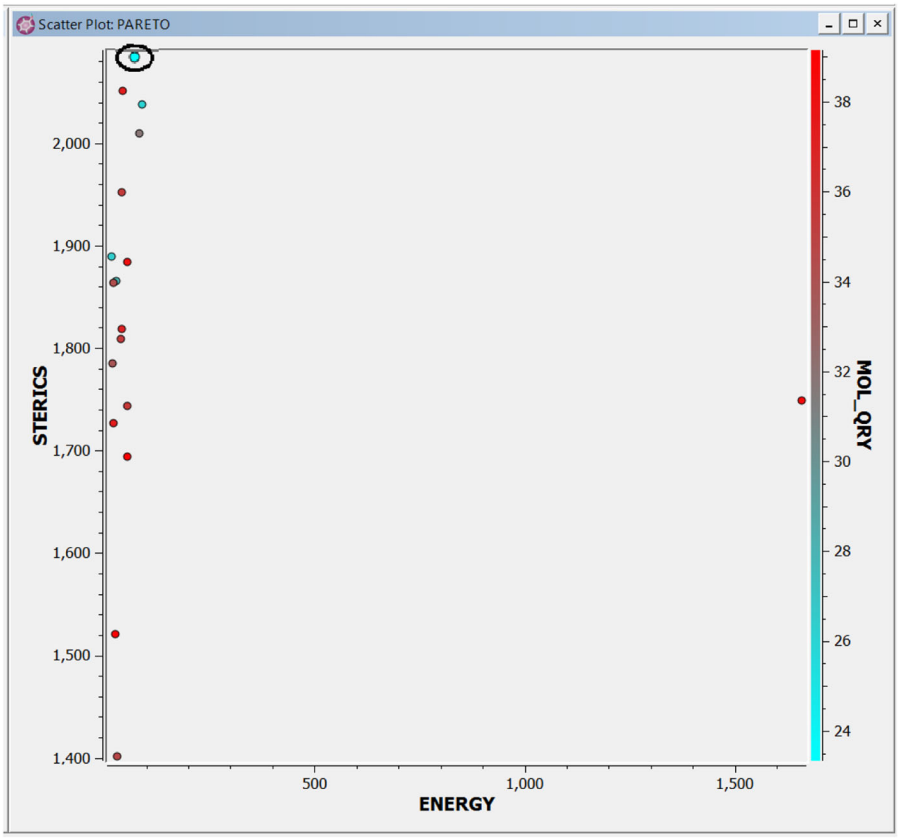

Fig. 4 Pareto scatter plot (energy vs. sterics) from 20 models, black circled model_18 was selected for further alignment of all compounds

H-pyrrol-1-yl)benzoic acid/4(1*H*-pyrrol-1-yl)benzoic acid in DMF medium using HBTU as a coupling agent and DIEA as a base to give *N*-(5-bromo-4-(4-substitutedphenyl)-thiazol-2-yl)-4-(2,5-dimethyl-1*H*-pyrrol-1-yl)benzamides (**6a–e**)/*N*-(5-bromo-4-(4-substitutedphenyl)-thiazol-2-yl)-4-(1*H*-pyrrol-1-yl)benzamides (**7a**,**b**). The reaction of 5-bromo-4-phenylthiazole with 2,5-dimethoxytetrahydrofuran in refluxing acetic acid yielded 5-bromo-4-phenyl-2-(1*H*-pyrrol-1-yl)thiazole (**8**).

Further, compounds **10** and (**11a–d**) (Scheme 2) were prepared by reacting 4-(2,5-dimethyl-1*H*-pyrrol-1-yl)benzoic acid (**9**) with substituted aromatic amines in the presence of diisopropyl ethylamine (DIEA) and 2-(1*H*-benzotriazole-1-yl)-1,1,3,3-tetramethyluroniumhexafluorophosphate (HBTU) as a catalyst. The synthesized compounds were isolated in pure form using column chromatography. The prepared derivatives were confirmed by spectral analysis.

FTIR, ^{1}H NMR, ^{13}C NMR, and mass spectral data were found to be in agreement as per the projected structures of all the molecules.

FTIR spectrum of **4b** showed an absorption band at 3304 cm^{-1} associated with the secondary amine (–NH) group and an absorption band of carbonyl group appeared at 1608 cm^{-1}. The ^{1}H NMR spectrum showed a characteristic

Table 4 GALAHAD score for all aligned molecules using MODEL_18

	MIC	ENERGY	STERICS	H_BOND	MOL_QRY
10	25	5.49	171.40	0.20	0.27
11a	12.5	14.82	548.10	0.90	0.27
4a	50	4.39	2109.50	41.90	0.16
4b	1.6	15.99	5686.60	41.90	0.16
4c	1.6	7.72	5859.60	41.90	0.16
4d	12.5	8.56	5081.40	59.10	0.16
4e	25	8.91	3957.20	41.90	0.16
4f	1.6	5.97	2804.20	41.90	0.16
6a	12.5	5.12	730.70	58.80	35.43
6b	1.6	6.96	5808.20	83.10	58.04
6c	1.6	5.08	3783.60	58.80	35.43
6d	3.12	120.46	5259.30	182.40	14.43
11b	1.6	6.64	419.80	0.90	0.27
6e	1.6	5.54	6288.10	215.20	58.04
7a	12.5	14.04	406.10	83.10	58.04
7b	6.25	6.84	1764.90	83.10	58.04
8	1.6	−1.21	1.30	0.00	0.00
11c	12.5	13.24	814.50	17.70	0.27
11d	12.5	21.86	481.60	1.20	0.27
3a	25	11.34	477.10	83.10	58.04
3b	1.6	9.23	2866.80	83.10	58.04
3c	3.12	10.69	2539.30	83.10	58.04
3e	1.6	10.50	3722.10	215.20	58.04
3d	1.6	16.58	4634.50	384.50	58.04

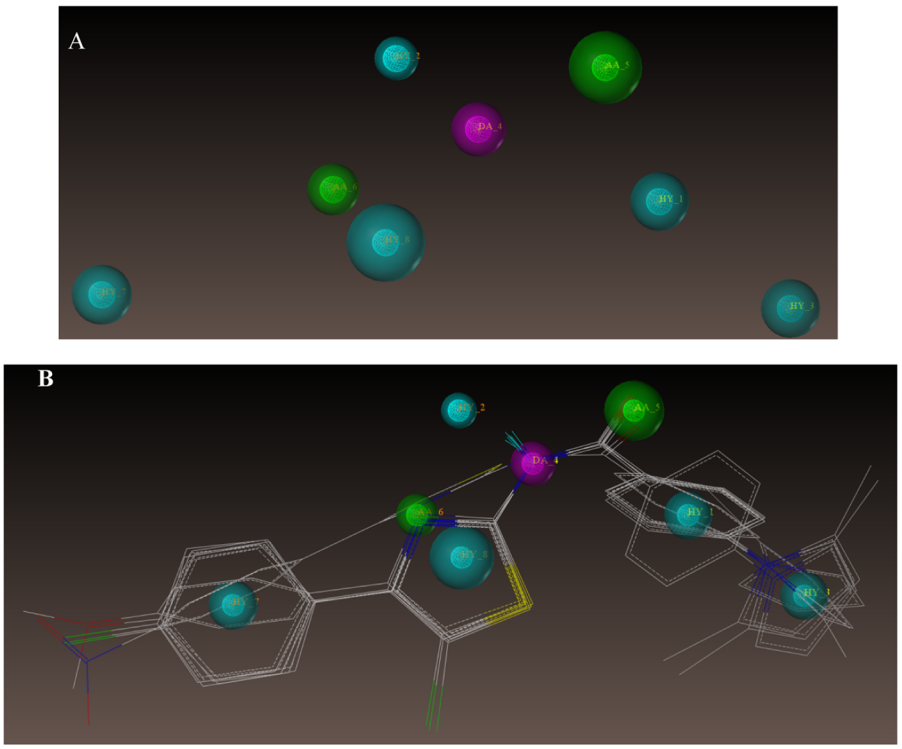

Fig. 5 **a** Final selected pharmacophore model and **b** molecular alignment for InhA receptor ligands (total of six compounds) containing acceptor atoms (green), positive nitrogen atom (red) and hydrophobes (cyan)

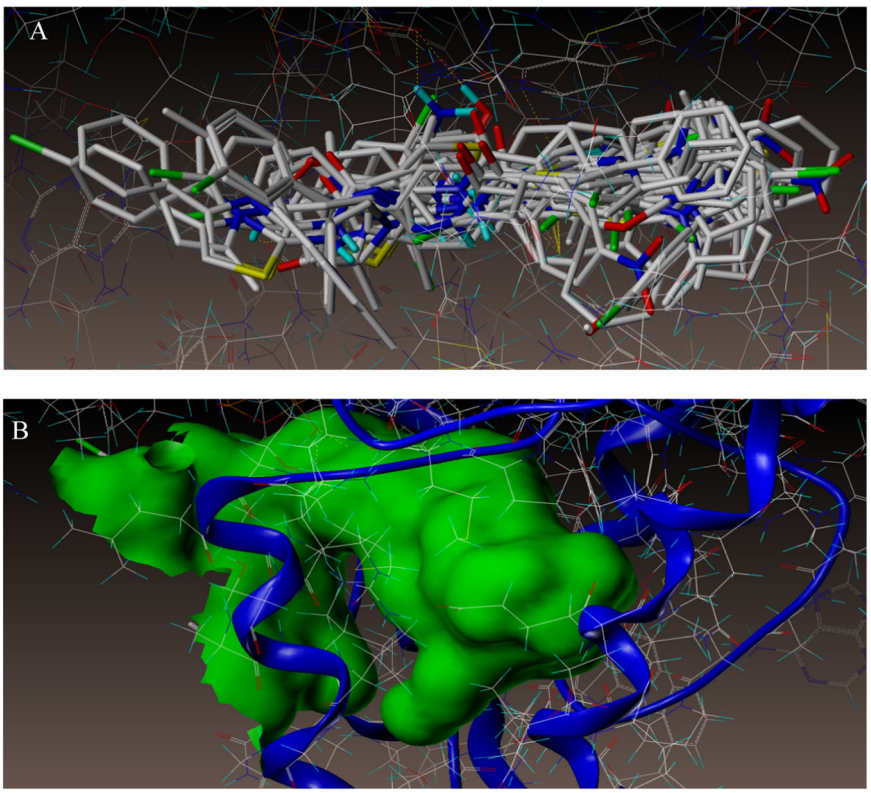

Fig. 6 Docked mode of all the synthesized compounds inside the proposed binding pocket of InhA

triplet signal for two protons of pyrrole at C_3 and C_4 positions and a singlet thiazole proton at C_5 position with the δ values of 5.94–5.82 and 7.54 ppm, respectively. The signals of aromatic protons (doublet, doublet of doublet, and multiplet) appeared between δ 7.53 and 8.14 ppm. In the ^{13}C NMR spectrum of compound **4b**, C = O carbon resonated at

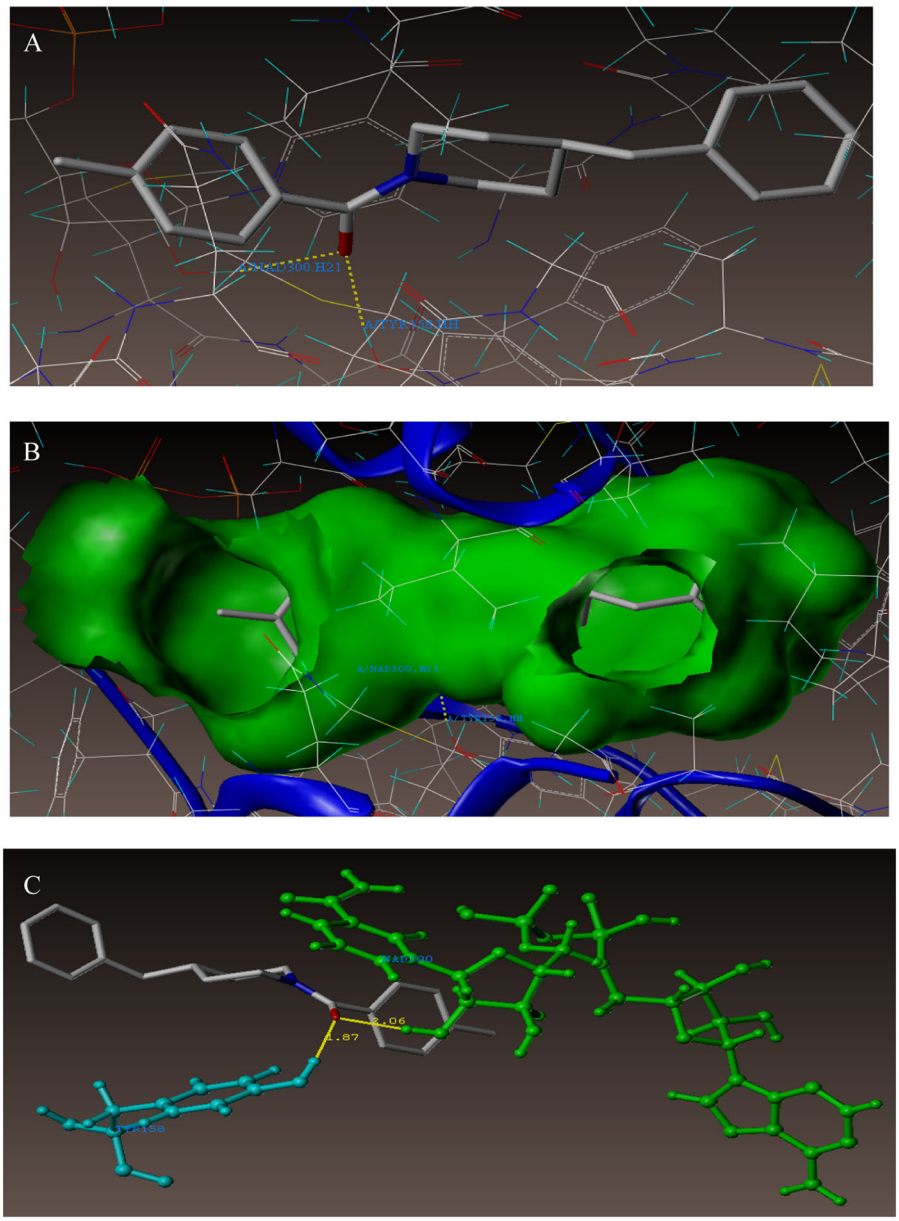

Fig. 7 **a** Docked mode of **2NSD_ligand**; **b** Inside the proposed binding pocket of InhA; **c** 3D docked view of the **2NSD_ligand**. Binding site residues; cyan colored Tyr 158 amino acid, green colored co-factor NAD+ and the molecule is colored according to atom type

δ of 168.66 ppm. The signals at δ of 121.37–146.33 ppm was due to aromatic carbons. Similarly, compound **6b** showed an absorption band at 3297 cm^{-1} associated with the secondary amine (–NH) group, while the absorption band of carbonyl group appeared at 1667 cm^{-1}. In the ^{1}H NMR spectrum, two protons of pyrrole at C_3 and C_4 positions appeared as characteristic singlet with the δ value 5.88 ppm. The signals shown between δ 7.50 and δ 8.10 ppm were attributed to aromatic protons, while the singlet signal at 2.01 confirms six pyrrolyl dimethyl protons at C_2 and C_5 positions. The ^{13}C NMR spectrum showed the signal at δ of 167.19 ppm, corresponds to the carbonyl group. All the aromatic carbons resonated in the expected values of δ of 124.23–134.01 ppm.

FTIR spectra of compounds **10** and (**11a–d**) showed absorption bands at 3223–3381 cm^{-1} owing to the NH group (2° amine) stretching and carbonyl group as strong bands in the region of 1635–1696 cm^{-1}, confirming the formation of compounds **10** and (**11a–d**). In the ^{1}H NMR spectra, the resonating signals of two protons of pyrrole at C_3 and C_4 positions are seen as triplet with the δ values ranging from 5.82 to 5.85 ppm. Aromatic protons appeared as doublet/doublet of doublet/doublet of triplet/triplet/triplet of doublet/multiplet around δ value of 6.79 and 8.12 ppm. The ^{13}C NMR spectra showed characterisitic signals of carbonyl carbon atom in the range of δ values of 165.13–167.36 ppm, whereas the remaining aromatic carbons appeared in the range of δ

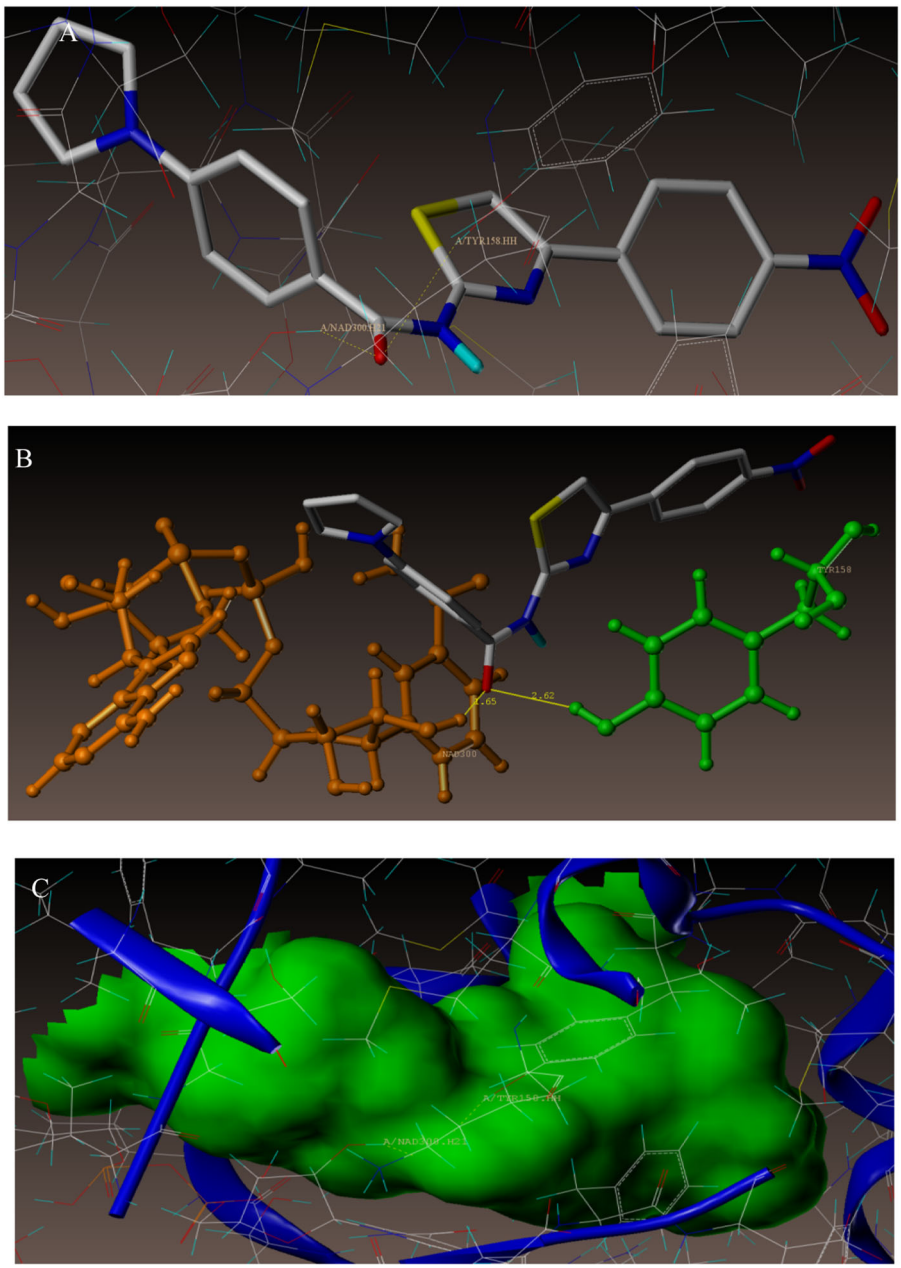

Fig. 8 **a** Docked mode of compound **3d**; **b** 3D docked view of compound **3d**. Binding site residues; green colored Tyr 158 amino acid, orange colored co-factor NAD+ and the molecule is colored according to atom type; **c** Inside the proposed binding pocket of InhA

106.61–144.73 ppm. Additionally, electron impact ionization (EI-MS) spectra that exhibited the molecular ion [M+] also confirmed the structures of the synthesized compounds.

Antimycobacterial and cytotoxicity studies

All the synthesized molecules were evaluated by determining minimal inhibitory concentration (MIC) on *M. tuberculosis* H37Rv strain (MTCC300) (Table 1). Pyrazinamide and streptomycin were used as reference drugs for comparison. The evaluated compounds exhibited activities against mycobacteria with the MIC values ranging from 1.6 to 50 µg/mL. Compounds **3b**, **3d**, **3e**, **4b**, **4c**, **4e**, **4f**, **6b**, **6c**, **6e**, **8**. **11b**, and **11c** inhibited mycobacterial growth very effectively compared to others in the series with a MIC value of 1.6 µg/mL.

The inclusion of bulky groups or halogen atoms increased the lipophilicity of the compound, while the mycobacterial cell wall is especially lipophilic, whose contributions of these lipophilic substituents played a significant role. Additionally, we have investigated the potential toxicity of eight selected pyrrole derivatives (**3b**, **3d**, **4c**, **4e**, **10**, **11b, 11c**, and **11d**) towards the mammalian

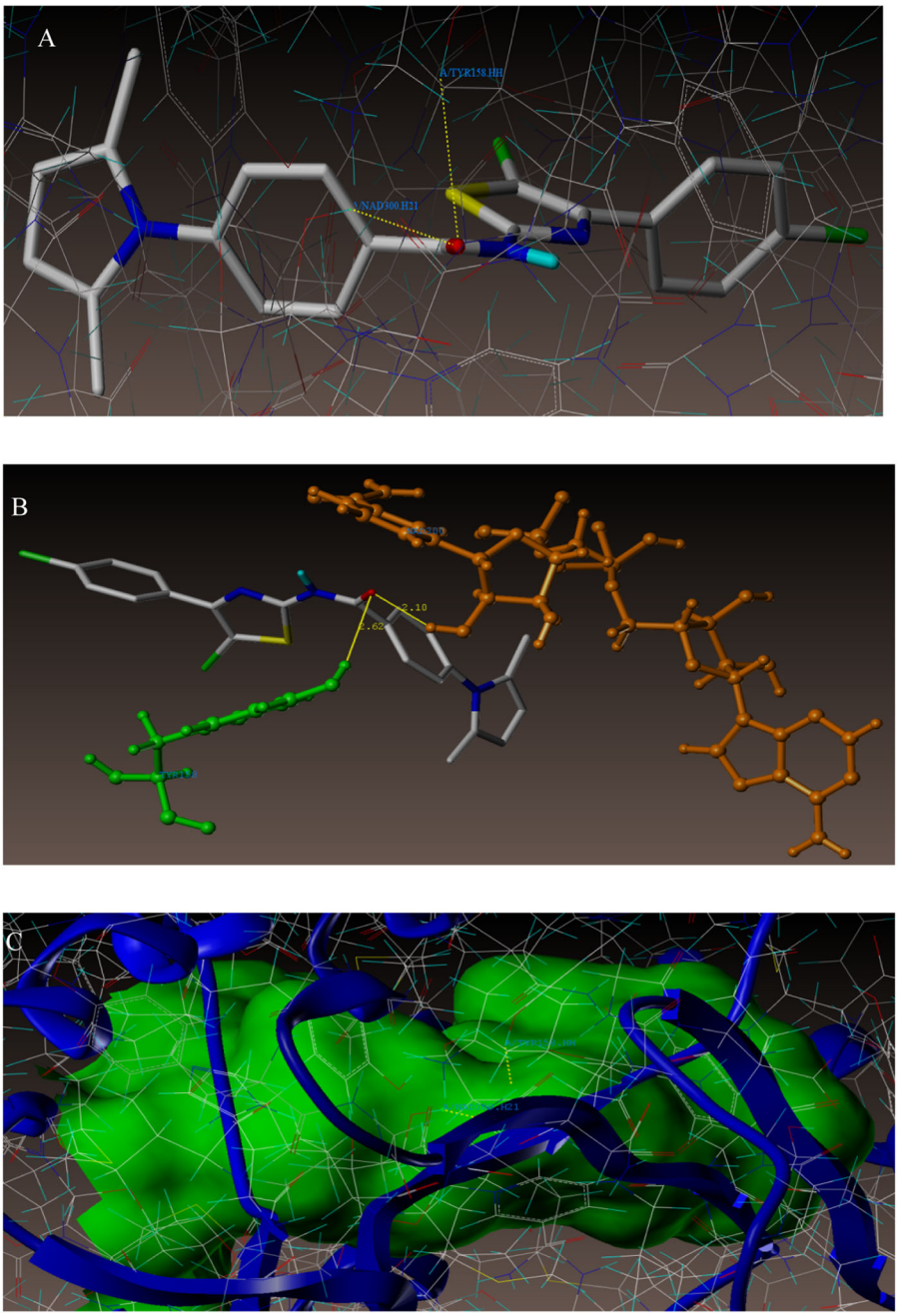

Fig. 9 **a** Docked mode of compound **6b**; **b** 3D docked view of compound **6b**. Binding site residues; green colored Tyr 158 amino acid, orange colored co-factor NAD+ and the molecule is colored according to atom type; **c** Inside the proposed binding pocket of InhA

Vero cell-lines and A549 (lung adenocarcinoma) cell-lines up to MIC values of 62.5 µg/mL were investigated. These tested molecules showed a modest cytotoxicity compared to the standard INH (see Table 2).

InhA inhibition assay

Twelve synthetic molecules were analyzed in vitro as potential InhA inhibitors from *M. tuberculosis* at 50 mM using triclosan as the reference drug by applying the generally accepted concepts and the results are displayed in Table 1. All the evaluated compounds gave related activities against InhA ranging between 12% and 38% of inhibition at 50 mM with the lowest values for compounds **10** and **11d** and the highest for compounds **4c** and **4e**.

Antibacterial activities

Antibacterial activity was also carried out for all the compounds against both Gram-positive bacteria (*S. aureus-MTCC096*) and Gram-negative bacteria (*E. Coli-MTCC443*). The antimicrobial results have shown that all

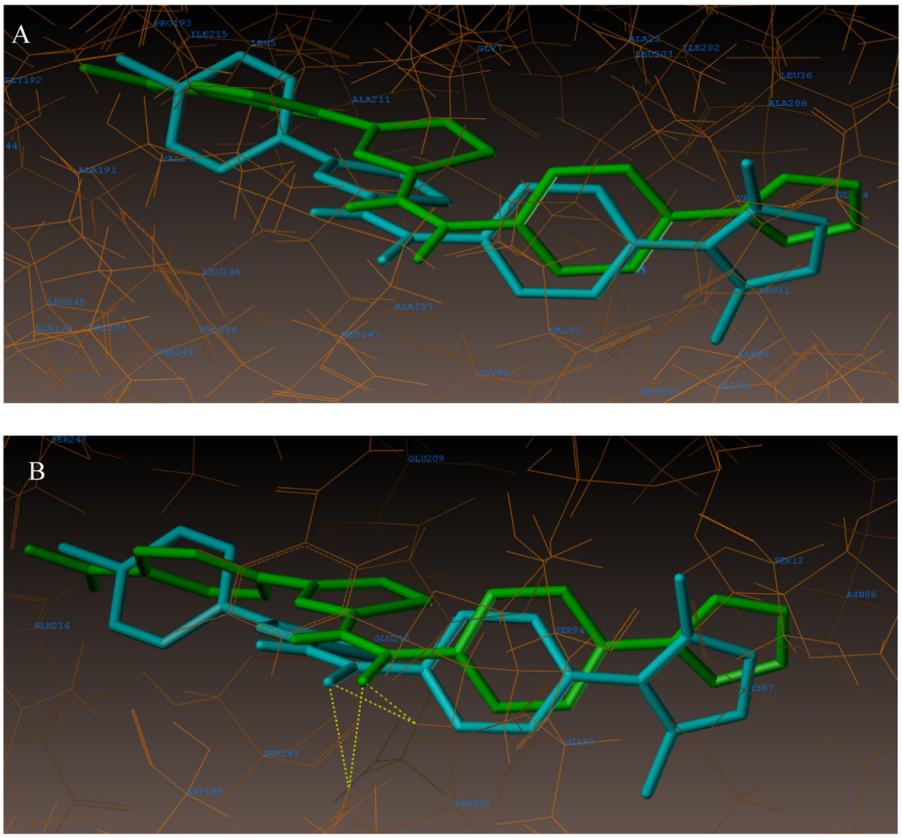

Fig. 10 **a** Hydrophobic amino acids surrounded to compounds **3d** (green color) and **6b** (cyan color). **b** Hydrophilic amino acids surrounded to compounds **3d** and **6b**

the compounds showed a moderate to good microbial inhibition in the range of MIC values of 1.6–50 µg/mL. These results suggest that the compounds are highly active towards Gram-positive bacteria *S. aureas* than the Gram-negative bacteria *E. coli*. The compounds **4c**, **4e**, **4f**, and **6b** have shown the highest activity against *E. coli* (MIC value of 1.6 µg/mL).

Pharmacophore results

In view of extensive applications of pharmacophore modeling in drug design research, the pharmacophore model was generated with six most active molecules with a MIC value of 1.6 µg/mL. Generally, the GALAHAD provides a total of 20 pharmacophore models ranked as per their fitness function. The generated models were ranked on the basis of energy profile, specificity value and Pareto rankings. As a result, the top-ranked MODEL_18 between all the 20 selected was used to understand the structural needs of the considered compounds, and was also taken into account for the final rigid alignment of the left over molecules. The description resulted from the final MODEL_18 are displayed in Fig. 5a, b, which contains five hydrophobes centered on two benzene rings, pyrrole ring as well as thiazole ring, two acceptor atoms center on oxygen atom (CONH linkage) and nitrogen atom (thiazole ring), as well as one positive nitrogen atom (CONH linkage). The pharmacophore model clearly exhibits the importance of hydrophobic phenyl, thiazole, and pyrrole rings with polar oxygen to confirm the anti-TB activity. The linking chain is also vital for exhibiting the activity.

Molecular docking

The active pocket was measured to be the location where 2NSD_ligand complexes with enoyl-ACP reductase in 2NSD. The 2NSD_ligand was re-docked to get its interactions and direction at the active site for the evaluation with other synthesized compounds (Fig. 6a, b). Docking studies with Surflex-Dock showed that the compound **3d** reside in the same binding site as that of 2NSD_ligand. The 2NSD_ligand has shown two H-bond interactions, the oxygen of carbonyl group makes two hydrogen bonds (Fig. 7a–c) with that of OH of the active site of NAD^+ ribose (2.06 Å) and with OH of the active site TYR158 (1.87 Å). The molecules **3d** and **6b** also bind in the similar manner i.e., oxygen atom of carbonyl group is responsible for H-bonding interactions, one bonding interaction with amino acid Tyr 158 and one more with co-factor NAD+ (Figs. 8a–c and 9a–c). Figure 10a, b exhibits hydrophobic and hydrophilic amino acids surrounded around molecules **3d** and **6b**.

Table 5 Surflex dock scores (kcal/mol) of pyrrole derivatives

Compounds	C score[a]	Crash score[b]	Polar score[c]	D score[d]	PMF score[e]	G score[f]	Chem score[g]
4PI	9.25	−0.93	1.54	−150.083	−63.091	−250.959	−46.922
3a	7.62	−0.53	1.18	−125.987	−84.693	−250.274	−43.687
10	6.93	−1.08	0.00	−128.036	−37.925	−230.226	−33.826
3c	6.61	−1.47	1.48	−136.790	−71.223	−255.580	−43.699
7a	6.47	−1.83	1.15	−138.107	−86.509	−269.607	−45.489
11d	6.14	−3.16	0.67	−127.964	−81.663	−279.021	−42.267
3d	5.29	−2.01	0.92	−136.362	−58.543	−253.306	−40.722
11c	4.96	−2.17	0.01	−138.049	−46.821	−234.920	−37.495
8	4.92	−0.94	0.00	−95.662	−70.793	−204.471	−36.643
3e	4.88	−4.37	0.00	−160.854	−41.194	−312.924	−41.741
11a	4.82	−1.86	0.01	−133.654	−36.897	−205.954	−35.242
TCL	4.55	−0.95	1.92	−115.813	−58.893	−181.923	−35.745
11b	4.26	−2.16	0.77	−152.168	−64.038	−235.404	−41.954
4e	4.26	−3.48	0.00	−141.933	−46.565	−258.198	−40.697
6d	4.18	−4.01	0.01	−168.982	−46.808	−295.678	−44.407
6a	4.03	−4.11	0.02	−159.142	−39.039	−296.074	−44.544
4c	3.97	−2.20	0.39	−132.946	−66.200	−264.862	−40.865
4b	3.81	−3.36	0.00	−121.191	−70.110	−252.681	−39.696
4a	3.61	−3.10	0.00	−112.664	−63.417	−269.857	−36.774
4d	3.44	−3.09	0.39	−118.026	−82.290	−266.253	−38.665
6b	3.34	−4.95	0.02	−167.251	−35.635	−304.477	−45.662
3b	3.29	−3.22	1.11	−136.719	−81.659	−243.112	−46.527
6c	3.28	−3.48	0.03	−144.721	−69.152	−286.852	−42.124
4f	3.19	−3.68	0.00	−137.692	−47.965	−250.815	−40.751
7b	2.95	−4.81	0.87	−150.398	−70.340	−288.449	−46.516
6e	2.25	−4.67	0.01	−143.402	−70.116	−272.019	−38.299

[a]CScore (Consensus Score) integrates a number of popular scoring functions for ranking the affinity of ligands bound to the active site of a receptor and reports the output of total score

[b]Crash-score revealing the inappropriate penetration into the binding site. Crash scores close to 0 are favorable. Negative numbers indicate penetration

[c]Polar indicating the contribution of polar interactions to the total score

[d]D-score for charge and van der Waals interactions between the protein and the ligand

[e]PMF-score indicating Helmholtz free energies of interactions for protein–ligand atom pairs (potential of mean force, PMF)

[f]G-score showing hydrogen bonding, complex (ligand–protein), and internal (ligand–ligand) energies

[g]Chem-score points for H-bonding, lipophilic contact, and rotational entropy along with an intercept term

The molecules displayed consensus score in the range of 7.62–2.25, demonstrating the requirement of all forces of interaction between the ligands and the enoyl ACP reductase enzyme. Charge and van der Waals interactions among the protein and molecules varied from −168.98 to −95.66. Helmholtz free energies of interactions for protein–ligands atom pairs ranged between −86.50 and −35.63 and its H-bonding, complex (ligand–protein), and internal (ligand–ligand) energies ranged from −304.47 to −181.92, while those values ranging from −46.92 to −33.82 indicate the ligands due to the presence of H-bonding, lipophilic contact, and rotational entropy. These scores suggest that the molecules selectively bind to the InhA in agreement with the reference 2NSD_ligand (Table 5).

Conclusions

New pyrrole derivatives have been synthesized that displayed interesting activities against InhA. These compounds were tested for inhibition of *M. tuberculosis* growth and antimicrobial activities against *S. aureus* and *E. coli*. Interestingly, molecules **3b, 3d, 3e, 4b, 4c, 4e, 4f, 6b, 6c, 6e, 8**, and **11c** showed the best activities with a MIC value of 1.6 μg/mL compared to other compounds. The potent

antimicrobial activities of the most active compounds were accompanied with a comparatively no evidence of cytotoxicity, indicating their nontoxic behavior. In addition, some compounds possess moderate InhA inhibition activities.

Pyrrole derivatives were further subjected to molecular docking and pharmacophore-mapping studies. The amino acid Tyr 158 and NAD^+ co-factor were found to be involved in H-bonding interaction and played a vital role in drug–receptor-binding interactions. On the other hand, amino acids (ILE202, ALA191, VAL92, GLY192, ALA211, MET103, ILE215, LEU207, LEU5, GLY7, LEU246, PRO193, ALA22, ALA157, LEU246, MET147) played hydrophobic interactions that are essential for inhibiting the enoyl ACP reductase enzyme. As per molecular modeling studies, these new inhibitors fitted well with the binding pocket of InhA in the same manner as those of TCL and 2NSD_ligands. Pharmacophores were generated using the GALAHAD Module of SYBYL 2.0 molecular modeling software, and contained two acceptor atoms, one positive nitrogen atom and five hydrophobic centers. The optimized pharmacophore model (MODEL_18) developed in this study showed the superior statistical parameters during the entire validation process. We believe that results of this study are useful as the guiding principles for designing and developing some putative new direct InhA inhibitors/antitubercular agents based on the suitable structural modifications of pyrrole scaffold.

Acknowledgements The authors acknowledge the financial support from Indian Council of Medical Research, New Delhi [ICMR letter Ref no. BIC/12(13)2014 dated 13-02-2017 (IRIS Cell no. 2014-2676)]. We are grateful to Dr. H.V. Dambal, President, S.E.T's College of Pharmacy, Dharwad, India for providing the facilities. We thank Dr. K.G. Bhat of Maratha Mandal's Dental College, Hospital and Research Centre, Belgaum, India for providing antitubercular and cytotoxic activities. Authors are grateful to the Director, SAIF, Panjab University, Chandigarh, Panjab, and IIT-Kanpur, India for providing some NMR and mass spectral data.

Compliance with ethical standards

Conflict of interest The authors declare that they have no conflict of interest.

References

Arora SK, Sinha N, Sinha RK, Uppadhayaya RS, Modak VM, Tilekar (2004) A program and abstracts of the 44th interscience conference on antimicrobial agents and chemotherapy (Washington, DC). American Society for Microbiology, Washington, DC

Biava M, Porretta GC, Poce G, Supino S, Deidda D, Pompei R et al. (2006) Antimycobacterial agents. Novel diarylpyrrole derivatives of BM212 endowed with high activity toward *Mycobacterium tuberculosis* and low cytotoxicity. J Med Chem 49:4946–4952

Caballero J (2010) 3D-QSAR (CoMFA and CoMSIA) and pharmacophore (GALAHAD) studies on the differential inhibition of aldose reductase by flavonoid compounds. J Mol Graph Model 29:363–371

Chimenti F, Bizzarri B, MaccioniE, Secci D, Bolosco A, Fioravanti R et al. (2007) A novel class of selective anti-*Helicobacter pylori* agents 2-oxo-2H-chromene-3-carboxamide derivatives. Bioorg Med Chem Lett 17:3065–3071

Chollet A, Mori G, Menendez C, Rodriguez F, Fabing I, Pasca MR et al. (2015) Design, synthesis and evaluation of new GEQ derivatives as inhibitors of InhA enzyme and *Mycobacterium tuberculosis* growth. Eur J Med Chem 101:218–235

Clark M, Cramer RD, Van Opdenbosch N (1989) Validation of the general purpose tripos 5.2 force field. J Comput Chem 10:982–1012

Deidda D, Lampis G, Fioravanti R, Biava M, Porretta GC, Zanetti S et al. (1998) Bactericidal activities of the pyrrole derivative BM212 against multidrug-resistant and intramacrophagic *Mycobacterium tuberculosis* strains. Antimicrob Agents Chemother 42:3035–3037

Dighe SN, Chaskar PK, Jain KS, Phoujdar MS, Shrinivasan KV (2011) A Remarkably high-speed solution-phase combinatorial synthesis of 2-substituted-amino-4-aryl thiazoles in polar solvents in the absence of a catalyst under ambient conditions and study of their antimicrobial activities. ISRN Org Chem, 11:434613

Franzblau SG, Witzig RS, McLaughlin JC, Torres P, Madico G, Hernandez A et al. (1998) Rapid, low- technology MIC determination with clinical *Mycobacterium tuberculosis* isolates by using the microplate Alamar Blue assay. J Clin Microbiol 36:6362–6366

Goto S, K. Jo K, T. Kawakita T, S. Mitsuhashi S, T. Nishino T, N. Ohsawa N et al. (1981) Method of minimum inhibitory concentration (MIC) determination. Chemotherapy 29:76–79

Guardia A, Gulten G, Fernandez R, Gómez J, Wang F, Convery M et al. (2016) N-Benzyl-4- ((heteroaryl)methyl)benzamides: a new class of direct NADH dependent 2-trans enoyl-acyl carrier protein reductase (InhA) inhibitors with antitubercular activity. Chem Med Chem 5:687–701

Gundersen LL, Nissen-Meyer J, Spilsberg B (2002) Synthesis and antimycobacterial activity of 6-arylpurines: the requirements for the *N*-9 substituent in active antimycobacterial purines. J Med Chem 45:1383–1386

Guner O Ed (2000) Pharmacophore perception, development, and use in drug design. International University Line, La Jolla, CA

Hantzsch A, Weber JH (1887) Ueber Verbindungen des Thiazols (Pyridins der Thiophenreihe). Ber Dtsch Chem Ges 20:3118–3122

Hoshino K, Ishida H, Omovskaya O, Dudley M et al. (2002) Japan Kokai Tokkyo Koho CODEN; JKXXAF JP 2002322054 A2 20021108. Chem Abstr 137:346134

Jain AN (1996) Scoring noncovalent protein-ligand interactions: a continuous differentiable function tuned to compute binding affinities. J Comput Aided Mol Des 10:427–440

Jain AN (2003) Surflex: fully automatic flexible molecular docking using a molecular similarity-based search engine. J Med Chem 46:499–511

Joshi SD, Dixit SR, Basha J, Kulkarni VH, Aminabhavi TM, Nadagouda MN et al. (2018) Pharmacophore mapping, molecular docking, chemical synthesis of some novel pyrrolyl benzamide derivatives and evaluation of their inhibitory activity against enoyl-ACP reductase (InhA) and *Mycobacterium tuberculosis*. Bio Org Chem 81:440–453

Joshi SD, Dixit SR, Kulkarni VH, Lherbet C, Nadagouda MN, Aminabhavi TM (2017) Synthesis, biological evaluation and in silico

molecular modeling of pyrrolyl benzohydrazide derivatives as enoyl ACP reductase inhibitors. Eur J Med Chem 126:286–297
Joshi SD, Dixit SR, More UA, Aminabhavi TM, Kulkarni VH, Gadad AK (2014) Enoyl ACP reductase as effective target for the synthesized novel antitubercular drugs: a-state-of-the-art. Mini Rev Med Chem 14:678–693
Josh SD, Vagdevi HM, Vaidya VP, Gadaginamath GS (2008) Synthesis of new 4-pyrrol-1-yl benzoic acid hydrazide analogs and some derived oxadiazole, triazole and pyrrole ring systems: a novel class of potential antibacterial and antitubercular agents. Eur J Med Chem 43(9):1989–1996
Joshi SD, Kumar D, Dixit SR, Tigadi N, More UA, Lherbet C et al. (2016a) Synthesis, characterization and antitubercular activities of novel pyrrolyl hydrazones and their Cu-complexes. Eur J Med Chem 121:21–39
Joshi SD, Kumar D, Dixit SR, Joshi AS, Aminabhavi TM (2016b) Drug resistanc antitubercular agents at the genetic level in mycobacterium Species: A road map to drug development for counteracting the resistance. Mini Rev Org Chem 13:262–280
Kalkhambkar RG, Kulkarni GM, Shivkumar H, Rao NR (2007) Synthesis of novel triheterocyclic thiazoles as anti-inflammatory and analgesic agents. Eur J Med Chem 42:1272–1276
Karuvalam RP, Haridas KR, Nayak SK, Guru Row TN, Rajeesh P, Rishikesan R, Suchetha Kumari N (2012) Design, synthesis of some new (2-aminothiazol-4- yl)methylester derivatives as possible antimicrobial and antitubercular agents. Eur J Med Chem 49:172–182
Masuda N, Moritomo A, Yamamoto O, Fujji M, Ohgami T, Kantani et al. (2005) Homocoupling of aryl iodides and bromides using a palladium/indium bimetallic system. Synth Commun 35:2305–2321
Menendez C, Gau S, Lherbet C, Rodriguez F, Inard C, Rosalia MP et al. (2011) Synthesis and biological activities of triazole derivatives as inhibitors of InhA and antituberculosis agents. Eur J Med Chem 46:5524–5531
Menendez C, Chollet A, Rodriguez F, Inard C, Pasca MR, Lherbet C et al. (2012) Chemical synthesis and biological evaluation of triazole derivatives as inhibitors of InhA and antituberculosis agents. Eur J Med Chem 52:275–283
Metzger JV, Katritky R, Rees CW, (1984) Comprehensive heterocyclic chemistry. Chemical and biochemical engineering: New materials and developed components, Pergamon, New York, 6:pp. 235–332
Powell MJD (1977) Restart procedures for the conjugate gradient method Math Program 12:241–254
Mosmann T (1983) Rapid colorimetric assay for cellular growth and survival: application to proliferation and cytotoxicity assay. J Immunol Methods 65:55–63
Pattan SR, Dighe NS, Nirmal SA, Merekar AN, Laware RB, Shinde HV, Musmade DS (2009) Synthesis and biological evaluation of some substituted amino thiazole derivatives. Asian J Res Chem 2 (2):196–201
Richmond NJ, Abrams CA, Wolohan PRN, Abrahamian E, Willett P, Clark RD (2006) GALAHAD: 1. Pharmacophore identification by hypermolecular alignment of ligands in 3D. J Comput Aided Mol Des 20:567–587
Shepphird JK, Clark RD (2006) A marriage made in torsional space: using GALAHAD models to drive pharmacophore multiplet searches. J Comput Aided Mol Des 20:763–771
Shiradakar MR, Murahari KK, Gangadasu HR, Suresh T, Kalyan CA, Panchal DR et al. (2007) Synthesis of new S-derivatives of clubbed triazolyl thiazole as anti-*Mycobacterium tuberculosis* agents. Bioorg Med Chem 15:3997–4008
Tripos Bookshelf 7. 3 (2014) Tripos International, St. Louis, MO, USA
Tripos International Sybyl-X 2. 0 (2012) Tripos International, St. Louis, MO, USA
Tropsha A (2005) Application of predictive QSAR models to database mining. In: Oprea T (Ed.) Chemoinformatics in drug discovery. Wiley-VCH, Weinheim
Villanova A (1985) National Committee for Clinical Laboratory Standards, Methods for dilution antimicrobial susceptibility for bacteria grown aerobically, approved standard. National Committee for Clinical Laboratory Standards
World Health Organization (2019) http://www.who.int/tb/publications/globalreport/2018/en/index.html
Zhao X, Yuan M, Huang B, Ji H, Zhu L (2010) Ligand based-pharmacophore model of *N*-aryl and *N*-heteroaryl piperazine alpha 1A-adrenoceptors antagonist using GALAHAD. J Mol Graph Model 29:126–136